Geological and geochemical implications of the genesis of the Qolqoleh orogenic gold mineralisation, Kurdistan Province (Iran)

Batoul Taghipour[1], Farhad Ahmadnejad[2*]

[1]Department of Earth Sciences, Faculty of Sciences, Shiraz University, Shiraz, Iran
e-mail: Taghipour@shirazu.ac.ir,
[2]Department of Earth Sciences, Faculty of Sciences, Shiraz University, Shiraz, Iran
*Corresponding author, e-mail: Farhad_sekerter@yahoo.com

Abstract

The Qolqoleh gold deposit is located in the northwestern part of the Sanandaj–Sirjan Zone (SSZ), within the NE–SW trending Qolqoleh shear zone. Oligocene granitoids, Cretaceous meta-limestones, schists and metavolcanics are the main lithological units. Chondrite-normalised REE patterns of the ore-hosting metavolcanics indicate REE enrichment relative to hanging wall (chlorite-sericite schist) and footwall (meta-limestone) rocks. The pattern also reflects an enrichment in LREE relative to HREE. It seems that the LREE enrichment is related to the circulation of SO_4^{2-} and CO_2-bearing fluids and regional metamorphism in the Qolqoleh shear zone. Both positive and negative Eu anomalies are observed in shear-zone metavolcanics. These anomalies are related to the degree of plagioclase alteration during gold mineralisation and hydrothermal alteration. In progressing from a metavolcanic protomylonite to an ultramylonite, significant changes occurred in the major/trace element and REE concentration. Utilising an Al-Fe-Ti isocon for the ore-hosting metavolcanics shows that Sc, Y, K, U, P, and M-HREE (except Eu) are relatively unchanged; S, As, Ag, Au, Ca, LOI, Rb and LREE are enriched, and Sr, Ba, Eu, Cr, Co and Ni decrease with an increasing degree of deformation. Based on geochemical features and comparison with other well-known shear zones in the world, the study area is best classified as an Isovolume-Gain (IVG) type shear zone and orogenic type gold mineralisation.

Based on the number of phases observed at room temperature and their microthermometric behaviour, three fluid inclusion types have been recognised in quartz-sulphide and quartz-calcite veins: Type I monophase aqueous inclusions, Type II two-phase liquid-vapour (L-V) inclusions which are subdivided into two groups based on the homogenisation temperature (T_h): a) L-V inclusions with T_h from 205 to 255°C and melting temperature of last ice (T_m) from –3 to –9°C. b) L-V inclusions with higher T_h from 335 to 385°C and T_m from –11 to –16°C. Type III three-phase carbonic-liquid inclusions (liquid water-liquid CO_2-vapour CO_2) with T_h of 345–385°C. The mean values of the density of ore-forming fluids, pressure and depth of mineralisation have been calculated to be 0.79–0.96 gr/cm³, 2 kbar and 7 km, respectively. The $\delta^{18}O_{water}$ and δD values of the gold-bearing quartz-sulphide veins vary from 7.2‰ to 8‰ and –40.24‰ to –35.28‰, respectively, which are indicative of an isotopically heavy crustal fluid and likely little involvement of meteoric fluid. The $\delta^{18}O_{water}$ values of the quartz-calcite veins have a range of –5.31‰ to –3.35‰, and the δD values of –95.65‰ to –75.31‰, which are clearly lower than those of early-stage quartz-sulphide-gold veins, and are close to the meteoric water line. Based on comparisons of the D–O isotopic systematics, the Qolqoleh ore-mineralising fluids originated from metamorphic devolatilisation of Cretaceous volcano-sedimentary piles. Devolatilisation of these units occurred either synchronously with, or postdates, the development of penetrative (ductile) structures such as shear zones and during overprinting brittle deformation.

Keywords: fluid inclusion, $\delta^{18}O$ and δD isotopes, rare earth and trace element mobility, Sanandaj-Sirjan Zone, Iran

1. Introduction

Orogenic gold deposits are related to collision settings and active orogenic belts (Bierlein et al., 2001). They formed during compressional to transpressional deformation processes at convergent plate margins in accretionary and collisional orogens (Groves et al., 1998, 2000; Goldfarb et al., 2001). These deposits are epigenetic and structurally controlled, and based on their depth of formation, are divided into epizonal, mesozonal, and hypozonal subtypes (Groves et al., 1998, 2000; Goldfarb et al., 2005).

Except for the Zartorosht and Muteh gold deposits, which are located in the southeastern and central parts of the Sanandaj-Sirjan Zone (SSZ) (Fig. 1), respectively, no major orogenic gold deposits have been recognised in Iran. Nevertheless, several gold occurrences have recently been explored in the northwestern SSZ (Fig. 2). Previous studies of the Qolqoleh gold deposit have outlined some aspects of gold mineralisation (Aliyari et al., 2009) and the

behaviour of major, trace and REEs during hydrothermal alterations (Aliyari et al., 2012).

Many researchers have investigated shear-zone formation and various aspects of elements mobility and volume/mass changes during mylonitisation (Sinha et al., 1986; O'Hara, 1988; Dipple et al., 1990; Selverstone el al., 1991; Goddard & Evans, 1995; Condie & Sinha, 1996; Hippertt, 1998; Kwon et al., 2009). Some investigations suggest that almost all major and many trace elements can be mobilised during mylonitisation (e.g., Dickin, 1988; O'Hara & Blackburn, 1989; Selverstone el al., 1991; Glazner & Bartley, 1991; Condie & Sinha, 1996; Rolland et al., 2003). REE geochemistry is often used to characterise protoliths of metamorphosed and highly altered rocks (e.g., Taylor & McLennan, 1985; Vance & Condie, 1987; Murray et al., 1990). However, these elements can also be mobilised during deformation and metamorphism (Dickin, 1988; O'Hara, 1990; Goddard & Evans, 1995; Condie & Sinha, 1996).

The behaviour of REE and Y is strongly decoupled from that of other elements (except U-Ta-Th-
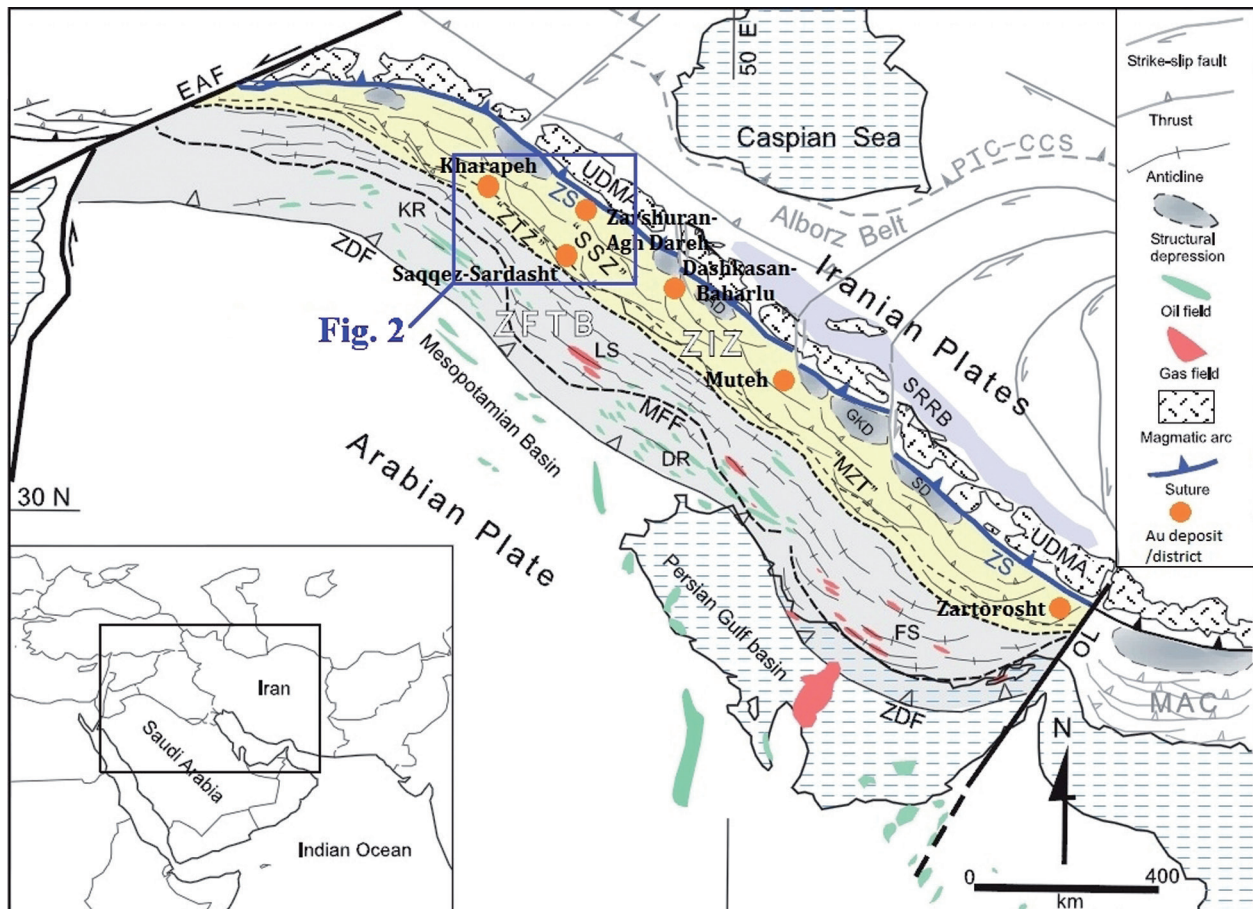

Fig. 1. Tectonic subdivision zones of the Zagros orogen, western Iran, and location of known gold deposits in the Sanandaj-Sirjan Zone (modified after Berberian, 1976; Eftekhar-Nezhad, 1981; Niromand et al., 2011).

Hf) in the shear zone (Rolland et al., 2003). Regarding REE mobility in shear zones, it is necessary to consider the mineralogical equilibria between fluids and REE-bearing minerals, as well as effects of pH, temperature, redox conditions and of potential ligands present in the mineralising fluid (Bau, 1991; Fourcade et al., 1989; Rolland et al., 2003). Precipitation and dissolution of REE-bearing minerals at various stages of shear zone development is an in-dicator of changes in fluid chemistry in the individual shear zone.

To study element behaviour during the deformation progress in shear zones, element distribution can be evaluated with Al-Ti-Fe isocon plots (Condie & Sinha, 1996). Based on the isocon method and volume or mass change during deformation, shear zones are classified into three groups: (1) volume-conservative (isovolume); (2) volume-loss,
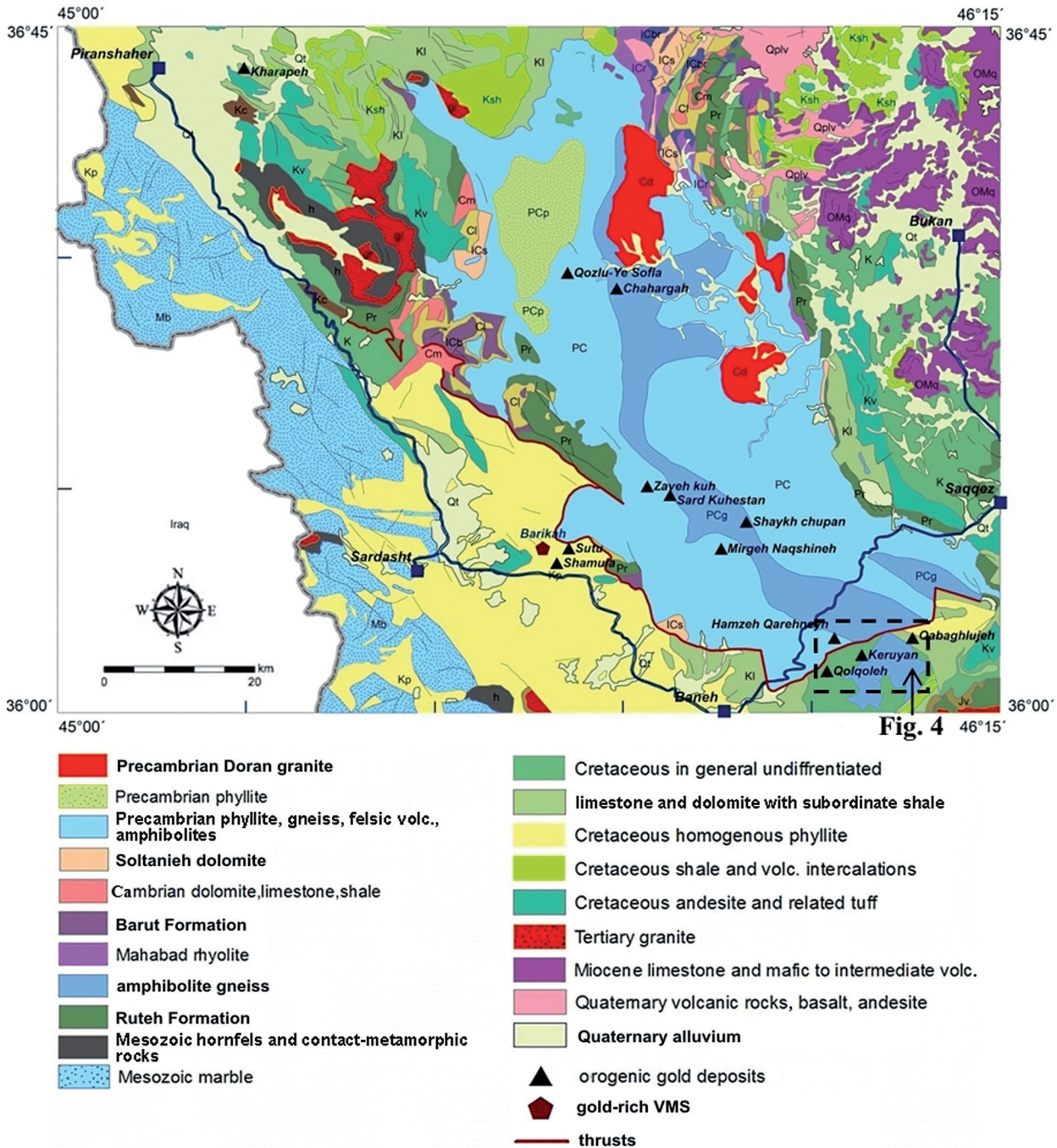

Fig. 2. Simplified geological map of the Saqqez-Sardasht-Piranshaher area (after Eftekhar-Nezhad, 1973) showing gold occurrences.

and (3) volume-gain (Condie & Sinha, 1996; Kwon et al., 2009).

This paper focuses on the geochemistry of trace elements and REE during transition from protomylonite to ultramylonite conditions in the Qolqoleh shear zone. The best-fit Al-Ti-Fe isocon method is used to determine chemical and volume change during mylonitisation and development of shear zone. Detailed fluid inclusion analyses and stable isotope data are used to determine possible sources of mineralising fluid, and to propose a model for the Qolqoleh shear zone evolution.

2. Methodology

A total of about ninety-five surface rock samples were collected for petrographical and geochemical investigations. Twenty fine microscopic thin sections were prepared for petrographical studies. Nine intrusive rocks were analysed for major and trace elements using X-ray fluorescence (XRF) (Philips PW2400, equipped with an Rh-tube) at the Kansaran Binalood laboratory, Pardis Science and Technology Park, Iran. The detection limit for the major oxides is about 0.01 wt%, but it varies for trace elements (in ppm): Nb (1); Th and Rb (2); Y and Ni (3); Cr, V and Zr (4); Sr (5); and Ba (10). In addition, 18 metavolcanics, chlorite-sericite schist (hanging wall) and meta-limestone (footwall) samples were analysed for trace and rare earth elements using inductively coupled plasma mass spectrometry (ICP-MS) in the ACME Analytical Laboratories Ltd., Vancouver, Canada. Microthermometric studies were carried out to investigate the nature and evolution of the mineralising fluids, and to determine physicochemical parameters of gold deposition with respect to the regional metamorphic and magmatic conditions. The fluid inclusion studies were carried out on 10 polished, thin-sectioned quartz specimens. These studies were carried on both concordant gold-bearing quartz-sulphide, and discordant quartz-calcite veins and veinlets. Microthermometric measurements were obtained on a Linkhan THM 600 heating/freezing stage with a temperature range of –196 to 600°C, mounted on a Zeiss-Olympus petrographic microscope at the Iran Mineral Processing Research Center and Esfahan University. The system was calibrated with synthetic fluid inclusions (Sterner & Bodnar, 1984) at temperatures −56.6°C, 0.0°C, and 374.1°C. To avoid decrepitation of the inclusions, freezing was carried out prior to heating. For all final melting temperatures of CO_2, precision is ±0.1°C. In this study, about 145 fluid inclusions were investigated by microthermometry. To minimise effects of post-entrapment modifications such as necking down and partial or total leakage, inclusions that have been affected by these phenomena, and those in very highly-deformed quartz grains and secondary inclusions were avoided. Ten quartz vein samples (concordant gold-bearing quartz-sulphide veins and discordant quartz-calcite veins) were selected for microthermometric measurements. The nature of inclusions, their contents (liquid-solid-gas), distribution patterns, types (primary, secondary, pseudosecondary), post-entrapment modification, shape, size and phase categories were studied and documented using a petrographical microscope at varying magnifications following the techniques outlined by Roedder (1984) and Touret (2001).

Four quartz samples were analysed for $\delta^{18}O$ and δD. The oxygen isotopic composition of two types of quartz was measured on O_2 evolved from laser-assisted fluorination and deuterium composition of inclusion fluids in both quartz vein types was measured on H_2. Handpicked sampling was carried out from both concordant gold-bearing quartz-sulphide veins and discordant quartz-calcite veins. Quartz from these veins was crushed into 0.1–0.5 mm grains. All isotope analyses were performed in the Cornell stable isotope laboratory at the University of Cornell, USA. The external precision and accuracy for both $\delta^{18}O$ and δD is ±0.2%. Results for $\delta^{18}O$ and δD are compared against the Vienna Standard Mean Ocean Water (V-SMOW).

3. Geological setting

During the Middle to Late Triassic, the Neo-Tethyan Ocean had opened up between Iran and Arabia, with two different platforms on either side (Berberian and King, 1981). The subduction of Neo-Tethyan oceanic lithosphere beneath the southwestern border of central Iran eventually led to suturing of the Iranian and Arabian continents (e.g., Berberian and King, 1981; Alavi, 1994), and subsequent continental convergence formed the Zagros Orogenic Belt (Fig. 1).

The Zagros orogen is part of the extensive Alpine–Himalayan orogenic belt that formed during collision of the northeastern margin of the Arabian continental plate with the central Iranian microcontinent in the Cretaceous-Cenozoic (Berberian & King, 1981; Alavi, 1994; Mohajjel et al., 2003). The northwestern boundary of the Zagros orogen is chosen to be the East Anatolian strike-slip fault in southeastern Turkey, and the southeastern boundary of the Zagros orogen is the Oman Line (Alavi, 2007). This orogen consists of three distinctive par-

allel tectonic zones from the northeast to southwest including (Fig. 1) 1) the Cenozoic Urumieh-Dokhtar magmatic (UDMA); 2) the Sanandaj-Sirjan Zone (SSZ), and 3) the Zagros fold belt (Alavi 1994, 2007; Mohajjel et al. 2003; Agard et al. 2005; Sheikholeslami et al. 2008; Niromand et al., 2011).

The Sanandaj-Sirjan Zone, which hosts Qolqoleh and other gold occurrences, covers a region of polyphase deformation, the latest reflecting the collision of the Arabian continent and the central Iranian microcontinent, and subsequent southward propagation of the fold-thrust belt (Alavi, 1994; Mohajjel et al., 2003, Sarkarinejad and Alizadeh, 2009). It is a major NW-SE trending structural zone that extends for more than 1,500 km length and ap-

proximately 200 km width to the northeast of the Zagros Thrust System and contains the metamorphic core of the Zagros continental collision zone in western Iran (Baharifar et al., 2004; Mohajjel et al., 2003; Sarkarinejad and Alizadeh, 2009). Different hypotheses have been proposed for the mechanism and exact timing of subduction and collision along this active margin (i.e., the Zagros orogen). These hypotheses can be classified into two groups according to the timing of initial subduction and continental collision (Fig. 3): 1) Many researchers believe that the initiation of oceanic subduction occurred in the Early to Late Cretaceous (Berberian & Berberian, 1981; Moinevaziri, 1985; Alavi, 1994) and continental collision occurred in the Late Cre-
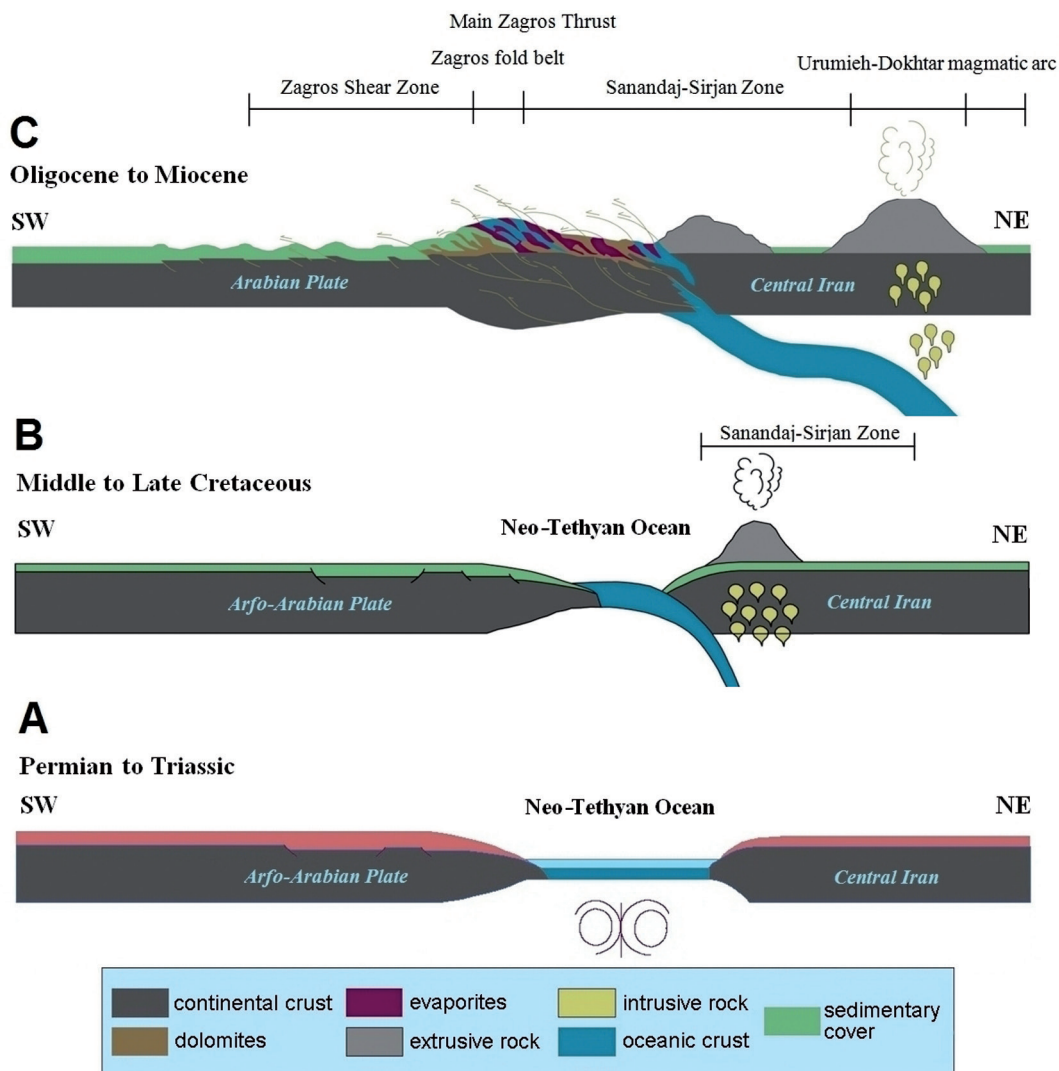

Fig. 3. Geotectonic model for the evolution of the northern part of the Sanandaj-Sirajan Zone (modified after Alavi, 1994; 2004; Agard et al., 2005; Niroomand et al., 2011).
   A – Neo-Tethys ocean opening in the Permian. The gold occurrences are formed in the western margin of central Iran; **B** – Subduction of Neo-Tethys oceanic crust started in the early Mesozoic, and the main part was subducted under central Iran by the end of the Cretaceous. Arc-related subduction was developed in the northern part of the Sanandaj-Sirjan zone; **C** – Final collision of the Arabian plate and central Iran in the Oligocene-Miocene (late Cenozoic).

taceous-Early Paleocene (Alavi, 1994, 2004), and 2) In contrast, some workers consider the timing of initial subduction to be Late Triassic-Early Jurassic (Agard et al., 2005; Arvin et al., 2007; Omrani et al., 2008) and suggest that the continental collision occurred in the Neogene (Berberian, 1983; Shahabpour, 2005). Deformed and mainly Mesozoic metasedimentary and metavolcanic rocks are located in the northwest to southeast of Iran (Mohajjel and Fergusson 2000) (Fig. 2). In addition to Jurassic-Eocene subduction-related intrusions in SSZ along the northeastern margin (e.g., the Urumieh–Dokhtar volcanic arc), there is a belt of Cretaceous flysch and volcanic rocks (Figs. 1, 2) in the northwestern part of the SSZ (Azizi and Moinevaziri 2009). Palaeozoic and Mesozoic rocks of the SSZ are metamorphosed and highly deformed in the Zagros orogenic belt (Alavi, 1994; Berberian, 1995). Eftekhar-Nezhad (1981) and Ghasemi & Talbot (2006) subdivided SSZ into two parts: 1) A belt of phyllite, metavolcanics and intrusive felsic rocks in the northwestern part of the SSZ, which were affected by deformation in the Late Cretaceous, and 2) Pre-Jurassic metamorphics and highly deformed post-Triassic sediments in the southeastern part. Recent studies by Azizi & Moinevaziri (2009) indicate that Cretaceous volcanic rocks are developed as a separate belt in the northern part of the SSZ between Nahavand and

Urumieh. This belt measures 15–20 km in width and 200–300 km in length, and extends in a NW–SE direction parallel to the main Zagros fault zone (Mohajjel et al., 2003; Azizi & Moinevaziri, 2009). According to Niromand et al. (2011), the Cretaceous metamorphosed volcano-sedimentary rocks of the Sardasht-Piranshahr-Saqqez zone host the gold deposits of the northwestern SSZ. These units underwent greenschist facies metamorphism (Fig. 2).

3.1. Geology of the Qolqoleh gold deposit

The Qolqoleh gold deposit is located at 36°08'08" N, 46°06'08" E in the northwestern part of the SSZ, 50 km southwest of Saqqez (Figs. 1, 2). This deposit is one of the gold occurrences of the Saqqez-Sardasht-Piranshaher gold-bearing zone. This zone has undergone deformation and greenschist facies metamorphism. Geochemical studies indicate that gold mineralisation in this zone is related to the ductile and brittle shear zones, which are suitable pathways for transportation and deposition of metals from ore-bearing fluids (Aliyari et al., 2007). Rock units exposed in the study area include granitoid intrusive (as widespread outcrops of gneiss and granite-gneiss), phyllite, meta-limestone, chlorite-sericite schist, and metavolcanics (Fig. 4). Meta-
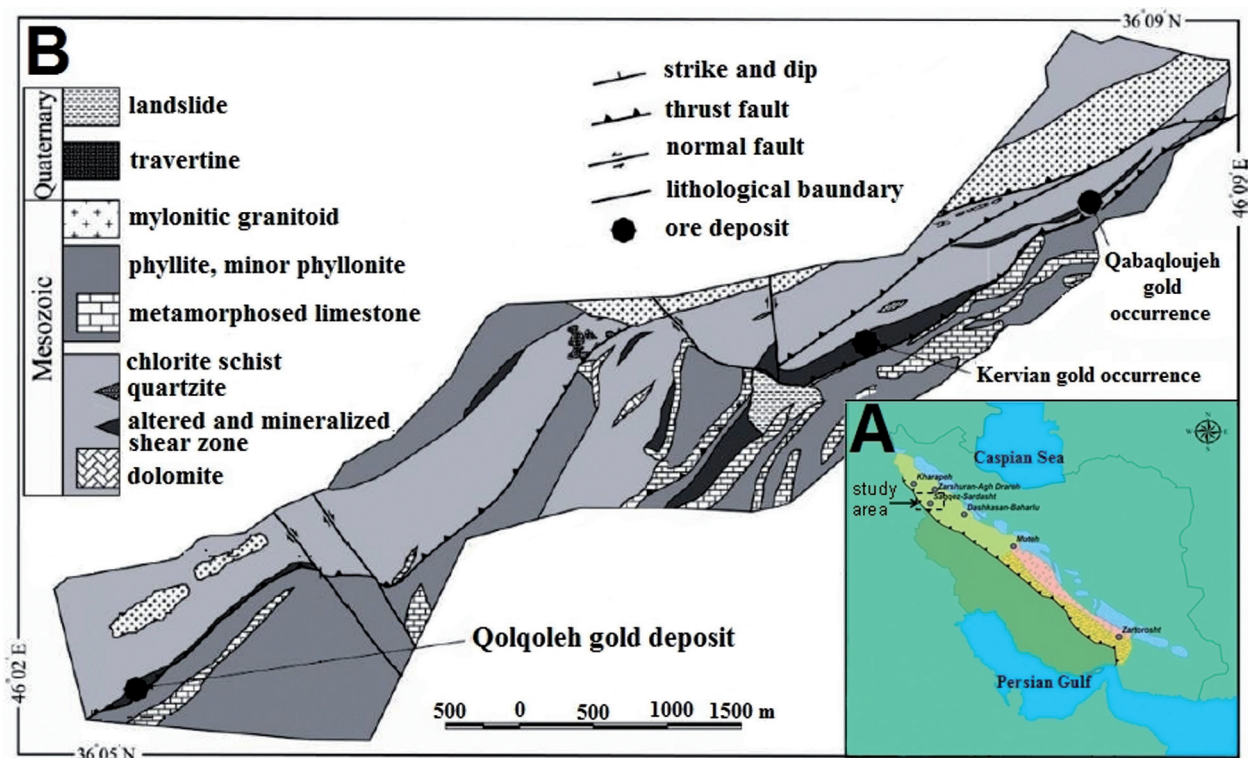

Fig. 4. A – Location of the study area within the Sanandaj-Sirjan metamorphic zone; **B** – Geological map of the study area showing location of major ore bodies and faults (modified after Mohajjel, 2000).

morphics, including chlorite-sericite schists, are the main component of hanging wall, whereas phyllite and meta-limestone constitute footwall. The area is affected by a NE–SW trending ductile-brittle shear zone. All rock units show different deformation intensity from less deformed to highly deformed. Propylitic, phyllic, and silicic are the main alteration zones in the area. Gold mineralisation is related to highly deformed silicified mylonite and ultramylonite units (Aliyari et al., 2009). The main mineralised zone is lens shaped, measuring about 2 km in length and 250 m in width.

Based on geometry, texture, and mineralogy, the quartz veins are classified into concordant and discordant types. The discordant quartz veins, as saddle shapes and/or as fracture fillings, were developed along extensional fractures in the fold limb propylitic, phyllic, and silicic are the main alteration zones. The concordant quartz veins host gold mineralisation, although some gold concentrations are present in discordant veins in the adjacent sulphidised altered wall rock.

There are three deformational stages (D_1, D_2 and D_3) in the structural history of the Sananda-Sirjan zone (Mohajjel et al., 2003). Mesoscopic fold and planar schistosity took place during D_1 deformation during the Late Jurassic-Early Cretaceous. D_2 deformation produced the shear zone trending NW-SE due to Afro-Arabian collision with the southwestern part of SSZ. The D_2 deformation episode led to the formation of dominant structures in the Qolqoleh (Mohajjel, 1997; Aliyari et al., 2009). Brittle to ductile shear zones formed as the D_3 deformation type in the Early Cenozoic.

4. Vein mineralogy

Field investigation shows two types of quartz veins: quartz-carbonate and quartz-sulphide.

4.1. Quartz-carbonate veins

These veins are characterised by low sulphide mineralisation. Mineralogy includes quartz (60 wt%), calcite (15 wt%), sericite-biotite (10 wt%), plagioclase (5 wt %), pyrite (<5 wt%), and chlorite and chalcopyrite (1–3 wt%). Quartz-carbonate veins cropped out mainly as dilation veins (Fig. 5A). The cross-cutting relationship suggests that silicification postdated carbonatisation (Fig. 5B). Relict patches of carbonates and rounded margins are common in the quartz matrix (e.g. Fig. 6A, B).
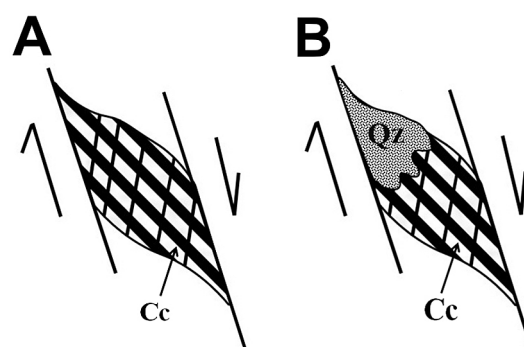

Fig. 5. Schematic sketch presenting the formation of a quartz-carbonate dilation vein.
A – Vein dilation and calcite replacement; **B** – Quartz replacement with some mineralisation.

4.2. Quartz-sulphide veins

Quartz-sulphide veins extend along mylonite induced foliations and host the greatest sulphide mineralisation in the area. These NW-SE trending veins are mostly widespread and occur in the mineralised parts of shear zones (Fig. 6C). The mineralogy includes quartz (70 wt%), plagioclase (10 wt%), biotite-sericite (10 wt%), and pyrite (> 5 wt%); chlorite and chalcopyrite are present as accessory minerals (Fig. 6D).

5. Geochemistry

Major and trace element geochemistry of nine samples from plutonic rocks (Table 1) suggests that the Qolqoleh gold deposit resulted from a sub-alkaline magma emplacement in a volcanic arc setting (Fig. 7A, B).

Except for a very high fluid/rock ratio (Michard, 1989), REEs with low solubility are relatively immobile during low-grade metamorphism, weathering and hydrothermal alteration (Rollinson, 1993). Some studies (e.g., Dickin, 1988; O'Hara, 1990; Glazner & Bartley, 1991) have shown that REE can be remobilised during deformation and metamorphism. According to Lottermoser (1992), very high fluid/rock ratios are necessary to make significant changes in the REE pattern of silicate-rich rocks during diagenesis and metamorphism.

The REE diagrams (Fig. 8) show enrichment in the shear zone ($\Sigma REE = 247$ ppm) relative to hanging wall and footwall units ($\Sigma REE = 143$ ppm and $\Sigma REE = 50$ ppm, respectively; Table 2). These patterns also reflect enrichment in LREE relative to HREE. In addition, it shows a stronger negative LREE slope compared to HREE. Both positive and
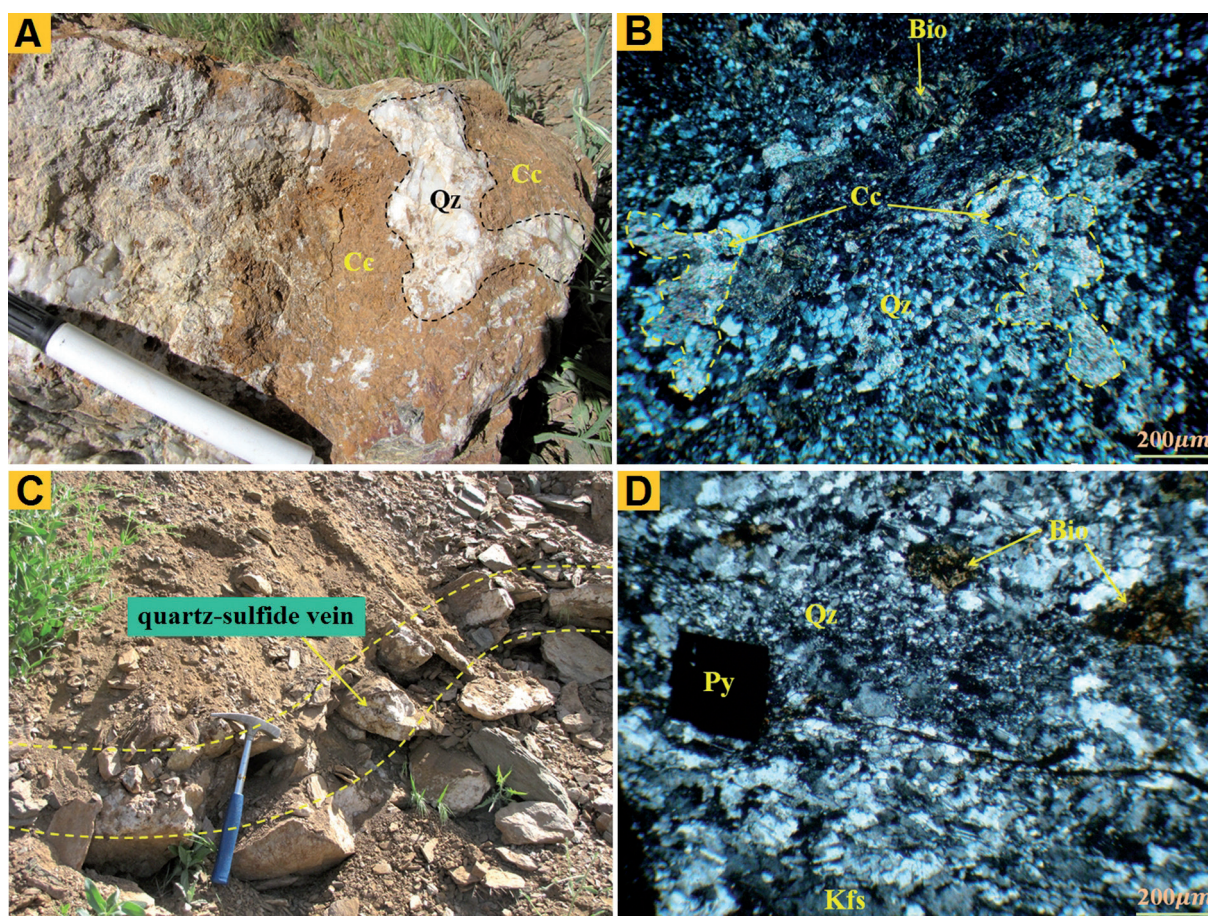
Fig. 6. A, B – Hand specimen and photomicrograph of quartz-carbonate vein; **C, D** – Quartz-sulphide veins along the Qolqoleh shear zone and photomicrograph of the same.

negative Eu anomalies are observed in the metavolcanics of the shear zone (e.g. Fig. 8A, B). Europium replaces Ca in plagioclase, so the negative and positive Eu anomalies correspond to the degree of plagioclase decomposition (Kikawada, 2001) or addition of plagioclase during hydrothermal alteration.

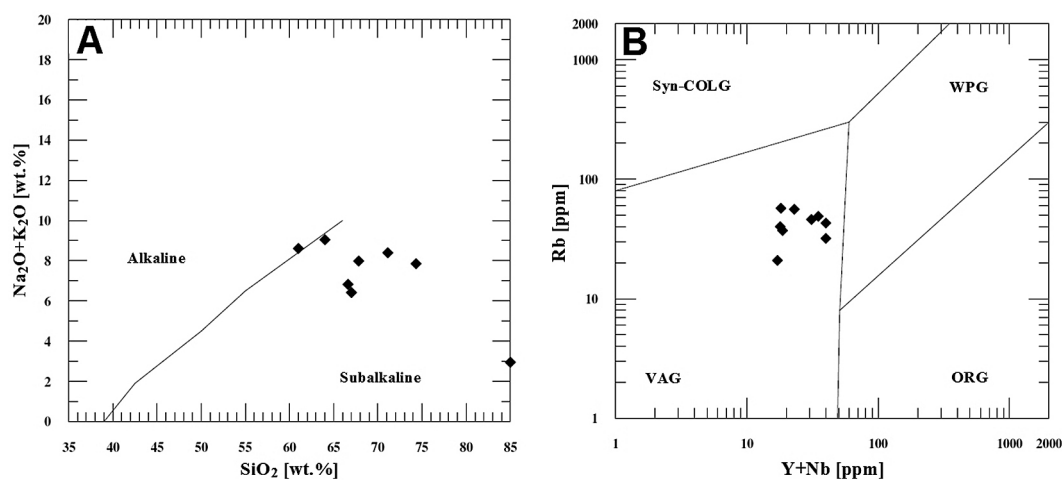Relative depletion of REE and absence of a Eu anomaly in the hanging wall (sericite-chlorite

Fig. 7. A – Discrimination diagram of alkaline-subalkaline series and position of samples studied (boundary after Irvine and Baragar, 1971); **B** – Rb *vs* (Y+ Nb) diagram for classification of granitoids and position of the Qolqoleh samples (boundaries after Pearce et al., 1984).

Table 1. Major and trace element composition of the intrusive body in the Qolqoleh deposit, Iran; <1 means below detection limit.

Samples	Gh.2.15	Gh.2.2	Gh.3.3	Gh.2.5	Gh.2.23	Gh.4.3	Gh.4.7	Gh.4.16	Gh.4.18
Samples	Gnd	Gn	Gn	Gnd	Dr	Gnd	Gn	Gn	Gn
SiO_2 (%)	67.13	85.06	85.82	64.11	61.93	66.61	74.32	71.12	67.83
TiO_2	0.41	0.38	0.39	0.42	0.37	0.62	0.58	0.95	0.71
Al_2O_3	13.35	8.53	7.1	14.32	17.01	17.70	14.17	14.36	16.94
Fe_2O_3	4.2	1.32	1.64	4.32	5.52	4.05	1.67	2.75	2.86
MnO	0.01	0.02	0.04	0.09	0.02	0.06	0.03	0.04	0.06
MgO	2.2	0.5	0.32	0.57	3.24	1.4	0.17	0.43	0.54
CaO	4.35	0.83	0.31	3.58	0.27	0.84	0.27	0.48	0.72
Na_2O	3.34	1.63	2.89	4.47	4.9	3.60	3.62	4.36	4.11
K_2O	2.9	1.32	1.62	4.58	3.71	3.32	4.23	4.03	3.87
P_2O_5	0.21	0.27	0.19	0.17	0.23	0.26	0.11	0.05	0.07
LOI	3.07	0.89	0.74	2.92	3.1	1.71	0.95	1.26	1.88
Total	98.96	100.28	100.67	99.31	99.90	100.07	100.12	99.83	99.54
Ba (ppm)	10.5	780	1018	870	1020	780	290	506	638
Rb	37.2	20.91	40.1	57.15	56	43	49	32	46
Sr	860	910	987	740	845	810	760	920	870
Zr	93	101	110	89	98	169	85	107	98
Y	8.71	10.1	12	7.2	11.01	26	24	21	15
Nb	10	7	6	11	12	14	11	19	16
Ga	20	21	23	19	20	18	20	29	23
Ag	1	1	1	<1	<1	1	1	1	1
Sn	2	1	3	2	1	2	1	<1	1
Ta	1.1	1.6	1.5	1.7	1.4	2.1	1.4	1.1	1.7
U	1.2	1.1	1.1	1.2	1.1	1.1	1	1.2	1.1
V	57	60	80	62	81	80	50	68	87
Ce	72	78	69	65	73	66	79	82	70
Th	9.8	7.2	8.5	4.7	7.3	15	11	2	7

schist) and footwall (meta-limestone) (Fig. 8C) are likely due to deformation and alteration processes. There is also the fractionation of LREE relative to HREE; $(La/Lu)_N$ ratios of metavolcanic, hanging wall and footwall samples are 12.77 (ppm), 12.98 (ppm), and 8.8 (ppm), respectively (Table 2).

5.1. Element mobility during mylonitisation

There are spatial and temporal relationships between the intensity of deformation and element distribution in the metavolcanic host rocks that have experienced various degrees of deformation. The highly deformed ultramylonitic units occur with ore-bearing zones in the inner parts of the Qolqoleh shear zone. High degrees of chloritisation, silicification and sulphidisation in the inner parts of the Qolqoleh shear zone are interpreted as reflecting an increased degree of deformation or changing conditions from weakly deformed rocks (protomy-

lonite, more than 50 wt% porphyroclast) to highly deformed and sheared rocks (ultramylonite, less than 10 wt% porphyroclast) in the metavolcanic units, whereas low-deformed protomylonitic units are found in the outer parts of the shear zone.

Significant changes in major, trace element, and REE chemistry have occurred during prograde deformation in the Qolqoleh metavolcanics. Ultramylonite rocks are characterised by a decrease in MgO and Na_2O, and an increase in SiO_2, CaO, and LOI. Relatively immobile components include P_2O_5, K_2O, Fe_2O_3, Al_2O_3, and TiO_2 (Fig. 9A).

In the Qolqoleh shear zone, U, Sc, Y, and Ba/Sr remained relatively constant throughout the deformation process, whereas Rb increased, and Th, Ba, and Sr decreased significantly during prograde deformation in the ultramylonites (Fig. 9B, C). In the ultramylonite unit, LREEs were enriched while HREEs remained relatively constant (Fig. 9D).

High gold concentrations in the metavolcanic units correlate with deformation intensity. There

Table 2. Concentration of major and trace element in the mylonite and ultramylonite metavolcanic units of the Qolqoleh shear zone. MMV: mylonitic metavolcanic; UMV: ultramylonitic metavolcanic; <1 means below detection limit.

Sample	GH 2.18	GH 2.22	GH 3.16	GH 4.6	GH 2.44	GH 2.47	GH 4.1	GH 3.12	GH 2.40
Sample	ML	ML	CSS	CSS	MMV	MMV	MMV	MMV	MMV
La (ppm)	12.03	13.2	27.21	28.9	39.18	35.24	38.69	33.49	41.4
Ce	21.1	16.7	57.43	58.8	74.23	69.5	69.67	54.6	73.18
Pr	2.2	1.7	6.5	6.7	8.93	8.31	8.26	7.54	9.17
Nd	8.4	7.5	28	28.2	37.1	35.66	37.59	32.85	39.81
Sm	1.9	1.62	5.8	5	8.3	7.3	6.9	6.2	8.2
Eu	0.7	0.51	1.9	1.6	4.9	3.72	4.82	4.3	5.2
Gd	2.1	1.7	5.6	5.2	8.9	6.58	6.83	5.13	7.21
Tb	0.4	0.24	0.75	0.6	1.46	1.02	0.98	0.78	1.14
Dy	2.1	1.4	4.1	3.6	6.72	4.51	6.04	4.8	5.74
Ho	0.4	0.32	0.7	0.6	1.3	0.9	0.97	0.81	1.1
Er	1.15	0.9	1.6	1.3	3.39	2.56	2.59	2.2	2.91
Tm	0.18	0.13	0.24	0.2	0.44	0.37	0.4	0.35	0.39
Yb	1.1	0.92	1.6	1.3	3	2.19	2.75	2.3	2.93
Lu	0.17	0.13	0.25	0.2	0.45	0.34	0.47	0.4	0.4
ΣREE	53.93	46.97	141.68	142.2	198.3	178.2	186.96	155.75	198.79
$(La/Yb)_N$	7.403	9.712	11.511	14.91	8.759	10.79	9.43	9.76	9.47
$(Eu/Eu)^*$	1.077	0.944	1.024	0.964	1.752	1.649	2.158	2.344	2.092
(Sm/Nd)	0.226	0.216	0.207	0.177	0.219	0.204	0.183	0.205	0.214

Sample	GH 4.19	GH 4.13	GH 4.10	GH 3.6	GH 3.7	GH 2.11	GH 2.29	GH 2.37	GH 4.20
Sample	MMV	UMV	UMV	UMV	UMV	UMV	UMV	UMV	UMV
La (ppm)	31.9	75.37	60.24	50.2	52.9	69.71	58.03	60.18	87.9
Ce	69.48	149.6	122.54	104.6	108.34	137.6	115.7	109.6	159.33
Pr	8.9	16.4	14.57	11.65	12.05	15.35	13.9	13.2	16
Nd	37.8	58.12	53.2	44.18	44.37	57.12	53.12	54	56.8
Sm	8.1	9.72	9.6	8.7	8.59	9.7	9.55	9.3	9.7
Eu	3.8	1.43	1.7	1.37	1.82	1.54	1.61	1.33	1.2
Gd	8.2	9.13	9.1	8.38	8.93	9.9	9.1	8.42	8.8
Tb	1.3	1.3	1.5	1.17	1.34	1.6	1.45	1.28	1.3
Dy	5.7	8	7.88	6.25	5.93	8.26	7.94	7.08	7.5
Ho	0.9	1.3	1.34	1.14	1.09	1.39	1.37	1.22	1.4
Er	1.9	3.69	3.6	3.31	3.1	3.76	3.81	2.9	3.3
Tm	0.27	0.47	0.51	0.42	0.43	0.47	0.53	0.35	0.43
Yb	2	2.87	2.97	2.59	2.56	2.83	2.4	2.71	2.5
Lu	0.3	0.37	0.42	0.48	0.41	0.45	0.39	0.4	0.39
ΣREE	180.55	337.77	289.17	244.44	251.86	319.68	278.9	271.97	356.55
$(La/Yb)_N$	10.69	17.61	13.6	13	13.86	16.52	16.3	14.89	23.582
$(Eu/Eu)^*$	1.433	0.466	0.558	0.493	0.638	0.48	0.53	0.462	0.398
(Sm/Nd)	0.214	0.167	0.18	0.19	0.193	0.169	0.179	0.172	0.17

is a positive correlation between $(La/Yb)_n$ ratio and gold content in the mylonitic and ultramylonitic metavolcanics (Fig. 10A). Au concentrations in the mylonite and ultramylonite units are 0.1–0.4 (ppm) and 1.3–4.5 (ppm), respectively (Tables 2, 3). The Sm/Nd ratio remains roughly constant during deformation (about 0.2) (Fig. 9D). In the shear zone there are also obvious changes of the Eu/Eu* ratio with deformation and alteration intensity (Eu/Eu*: 1.43–2.34 ppm in mylonite zone, 0.39–0.63 ppm in ultramylonite zone). Mylonitic zones are characterised by a positive Eu anomaly (Eu/Eu* > 1) and lower gold content (Au = 0.1–0.4 ppm), whereas ultramylonite units show a negative Eu anomaly (Eu/Eu* < 1) and higher gold content (Au = 1.3–4.5 ppm) (Tables 2, 3; Figs. 9D, 10B).
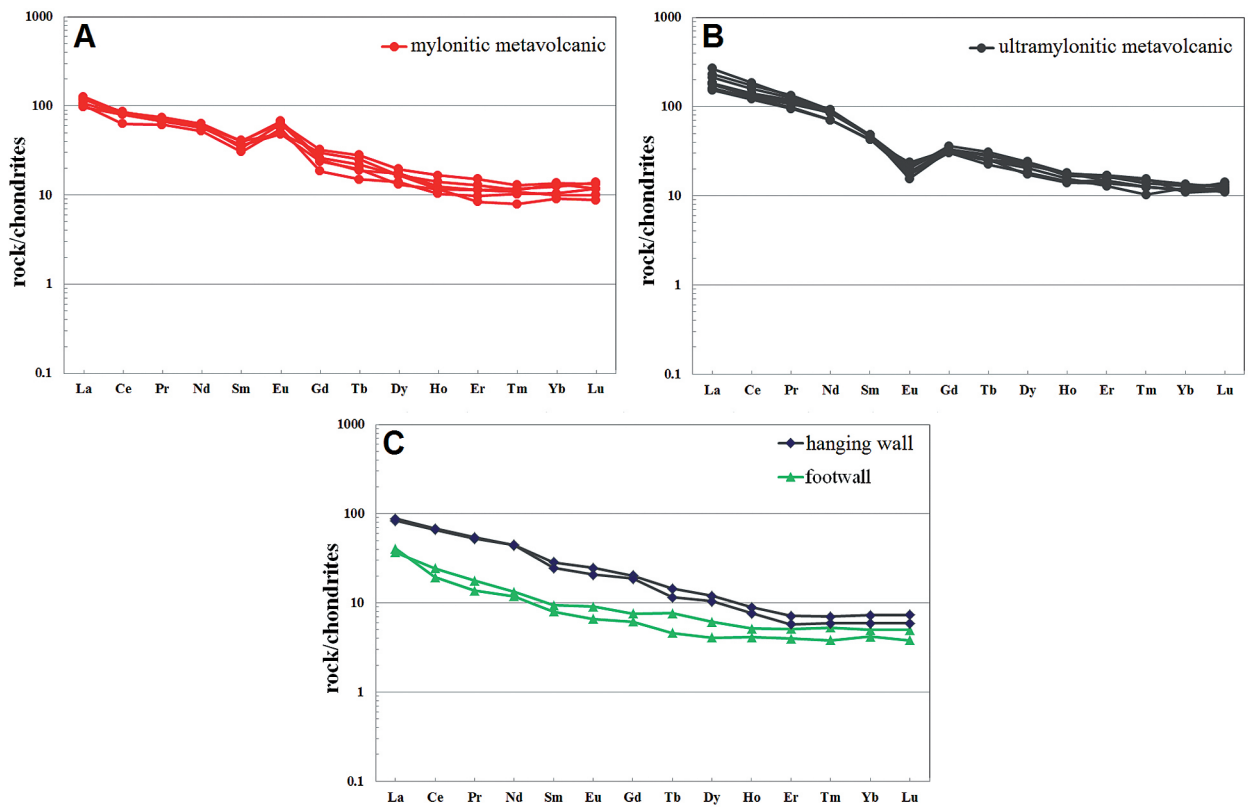
Fig. 8. The REE dispersion pattern in metavolcanic rocks of the Qolqoleh shear zone.
A – Mylonite; **B** – Ultramylonite; **C** – Hanging wall (sericite-chlorite schist) and foot wall (meta-limestone). All data are normalised to the Nakamura (1974) chondrite.
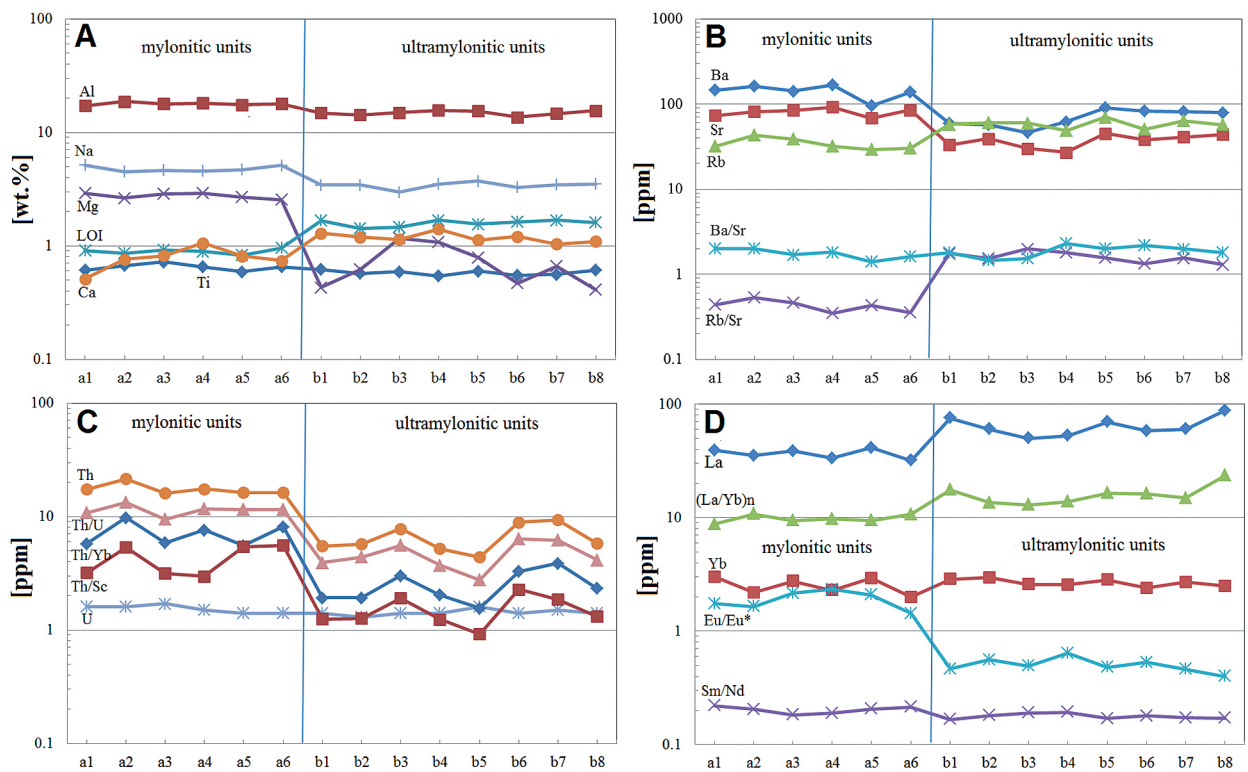

Fig. 9. Distribution patterns: **A** – major elements; **B** – HFSE; **C** – LILE; **D** – REE in mylonitic and ultramylonitic units. a1-a6 are samples from mylonitic units; b1-b8 from ultramylonitic units.

Table 3. Concentration of rare earth elements in the hanging wall, foot wall and mineralised shear zone of the Qolqoleh deposit. ML: meta-limestone; CSS: chlorite-sericite schist; MMV: mylonitic metavolcanic; UMV: ultramylonitic metavolcanic; <1 means below detection limit.

Sample	GH 2.44	GH 2.47	GH 4.1	GH 3.12	GH 2.40	GH 4.19	GH 4.13
Sample	MMV	MMV	MMV	MMV	MMV	MMV	UMV
Si (%)	64.58	62.84	64.35	64.57	64.81	65.2	70.8
Al	17.2	18.7	17.9	18	17.5	17.8	14.8
Fe	4.8	4.92	5.02	4.75	4.65	3.25	4.31
Ti	0.61	0.67	0.72	0.65	0.59	0.65	0.62
Ca	0.51	0.76	0.82	1.06	0.81	0.74	1.29
Na	5.15	4.51	4.62	4.57	4.7	5.1	3.43
K	2.9	3.13	2.64	2.57	2.47	3.18	2.81
Mg	2.91	2.64	2.88	2.9	2.68	2.55	0.43
P	0.31	0.45	0.42	0.43	0.39	0.37	0.32
LOI	0.91	0.86	0.92	0.89	0.83	0.96	1.67
Co (ppm)	29.1	23.7	25.4	33.3	28.6	24.7	13.4
Sc	5.4	4	5.1	5.9	3	2.9	4.4
Y	34.7	37.4	31.5	37	35.3	34.1	38.5
Rb	32	43.2	38.6	32	29.3	30.2	57.7
Cr	28	21	29	18	19	17	13
Ni	30	16	28	29	19	20	16
As	15	6.2	7.3	5.7	24	1.1	50.5
Pb	5	13	9	14	11	8	53
U	1.6	1.6	1.7	1.5	1.4	1.4	1.4
Zn	118	109	131	122	94	91	194.4
Ag	0.2	0.3	0.4	0.6	0.3	0.5	1.1
S	0.04	0.04	0.04	0.04	0.04	0.04	0.17
Sb	0.14	0.11	0.15	0.14	0.13	0.17	0.34
Bi	0.05	0.05	0.04	0.06	0.06	0.05	0.18
Au	0.3	0.4	0.1	0.3	0.3	0.2	2.9
Ba	146	161	142	167	95	138	58.99
Sr	73	81	84	92	68	85	33
Cu	20.3	12.7	21.2	19.4	17.9	17.6	34.2
Th	17.3	21.4	16.1	17.5	16.2	16.2	5.5
Rb/Sr	0.438	0.533	0.459	0.347	0.43	0.355	1.748
Ba/Sr	2	1.987	1.69	1.815	1.397	1.623	1.787
Th/U	10.812	13.375	9.47	11.666	11.571	11.571	2.87
Th/Yb	5.766	9.771	5.854	7.6	5.529	8.1	1.916
Th/Sc	3.203	5.35	3.156	2.966	5.4	5.586	1.25

5.2. Calculation of chemical changes

Although changes in element concentration with increasing degree of deformation in shear zones have been well documented in the literature (Newman & Mitra, 1993; Goddard & Evans, 1995; Ingles et al., 1999; Hippertt, 1998; Kwon et al., 2009), it is necessary to consider rock densities in order to identify element losses, gains, and changes in rock volume (Condie & Sinha, 1996). Based on Gresen's equation (1967), Grant (1986) developed an isocon diagram method for mass-balance analysis. As

Table 3. continued.

Sample	GH 4.10	GH 3.6	GH 3.7	GH 2.11	GH 2.29	GH 2.37	GH 4.20
Sample	UMV	UMV	UMV	UMV	UMV	UMV	UMV
Si (%)	71.16	71.34	70.4	69.75	72.06	70.44	70.14
Al	14.3	14.9	15.6	15.4	13.6	14.6	15.5
Fe	5.33	3.9	5.18	4.5	4.53	4.3	4.62
Ti	0.57	0.59	0.54	0.6	0.55	0.56	0.61
Ca	1.19	1.14	1.4	1.12	1.21	1.04	1.09
Na	3.44	2.97	3.5	3.72	3.28	3.46	3.5
K	2.15	1.93	2.21	2.75	2.86	2.77	3
Mg	0.62	1.17	1.08	0.79	0.47	0.66	0.41
P	0.3	0.28	0.29	0.26	0.28	0.29	0.315
LOI	1.42	1.46	1.68	1.55	1.63	1.68	1.6
Co (ppm)	9.3	16.1	12.2	12.6	16	15.3	10.1
Sc	4.5	4.1	4.2	4.8	3.9	5	4.4
Y	37.2	34.3	37.1	33.2	35.8	35.6	33.7
Rb	60.1	59.5	48.6	70	50.7	63.4	57
Cr	10	15	12	10	14	14	16
Ni	14	18	15	14	16	13	18
As	69.4	48.9	108	123.1	55	63	67.3
Pb	56	46	37	29	19	25	24
U	1.3	1.4	1.4	1.6	1.4	1.5	1.4
Zn	397	174	280.8	266	203	183	228.15
Ag	3	2.2	0.8	0.9	1.8	0.7	2
S	0.18	0.44	0.1	0.25	0.22	0.1	0.2
Sb	0.4	0.39	0.4	0.38	0.41	0.44	0.48
Bi	0.17	0.22	0.18	0.23	0.2	0.18	0.24
Au	1.3	2.7	1.4	1.9	4.5	3.1	3.6
Ba	57	46	62	90	83	81	79
Sr	39	30	27	45	38	41	44
Cu	41.4	38.3	43.4	53.7	35.8	51.6	36.5
Th	5.7	7.8	5.2	4.4	8.9	9.3	5.8
Rb/Sr	1.541	1.983	1.8	1.555	1.334	1.546	1.295
Ba/Sr	1.461	1.533	2.296	2	2.184	1.975	1.795
Th/U	4.384	5.571	3.714	2.75	6.357	6.2	4.142
Th/Yb	1.919	3.011	2.031	1.554	3.284	3.875	2.32
Th/Sc	1.266	1.902	1.238	0.916	2.282	1.86	1.318

Kwon et al. (2009) indicated, identification of 'immobile' elements is an important step because improper choice will lead to erroneous results.

The Al-Ti-Fe isocon (Grant, 1986, 2005; Condie & Sinha, 1996) is used to investigate element behaviour in the Qolqoleh shear zone. The best-fit isocon closely approximates the constant Al-Ti-Fe isocon, but this is distinct from the isocons corresponding to either constant volume or constant mass. Based on the Al-Ti-Fe isocon diagram of metavolcanics, Si, S, Ca, As, Zn, Cu, Au, Ag, Sb, Bi, Pb, Rb, LOI, and LREE show enrichment, whereas Sr, Ba, Na,
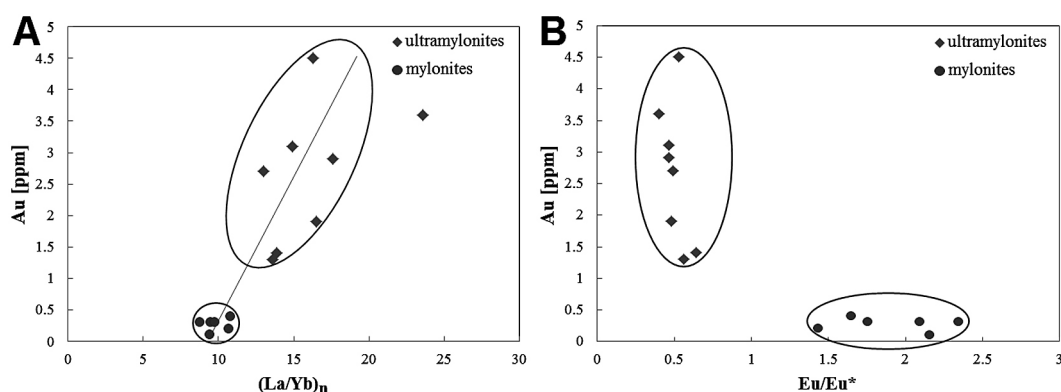
Fig. 10. Chondrite-normalised scatter diagrams for Au *vs* (La/Yb)$_n$ and Au *vs* Eu/Eu* in altered mylonitic metavolcanics and ultramylonitic metavolcanics.
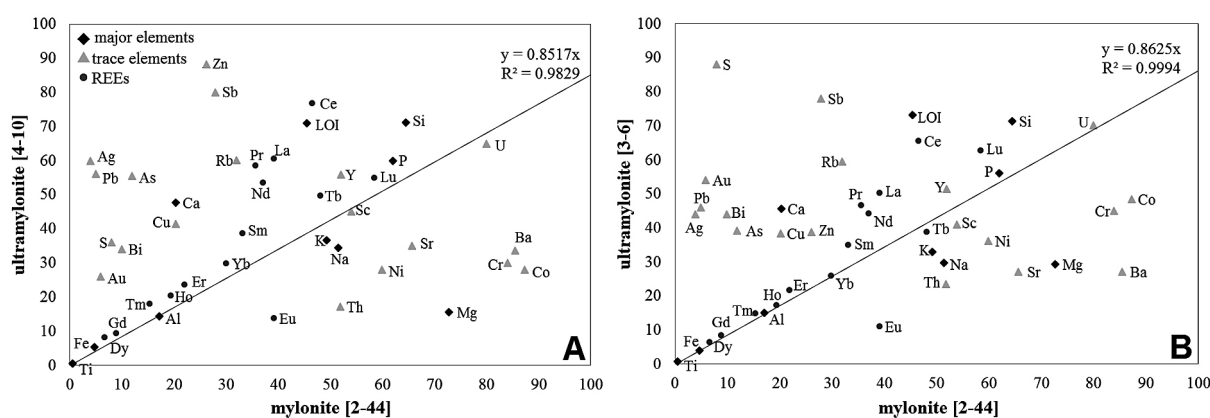

Fig. 11. Isocon diagrams in mylonites *vs* ultramylonites of the Qolqoleh shear zone. Sample numbers in square brackets

Eu, Mg, Th, Cr, Co, and Ni show depletion during prograded/prograding deformation (Fig. 11). Relatively immobile elements include Al, Ti, Fe, Sc, Y, K, U, P and HREE (except Eu). An increase in Si, S, Zn, Pb, and Cu is consistent with sulphide, sericite and silicic alterations in the Qolqoleh shear zone. It seems that these elements precipitated during hydrothermal alteration by Si-bearing fluids, which contained bi-sulphide complexes in highly deformed zones. The occurrence of pyrite and galena corresponds to the enrichment of Au, Sb, As, and Ag in this unit. The increase in Ca and LOI is related to hydrous minerals (e.g. muscovite and epidote) in ultramylonites. Mg, Sr, Na, and Ba depletion is followed by decomposition of biotite and feldspar minerals during mylonitisation (Sinha et al. 1986; Condie and Sinha 1996). In addition, other elements such as Cr, Ni, and Co have been depleted with increasing deformation intensity. Based on Rollinson (1993), these elements are relatively immobile, and may be mobile on a local scale (McCuaig & Kerrich 1998).

5.3. Classification of the Qolqoleh shear zone

Based on changes in volume or mass during deformation, shear zones are classified into three types (O'Hara, 1988; O'Hara & Blackburn, 1989; Selverstone et al., 1991, Bailey et al., 1994; Kwon et al., 2009): 1) Isovolume types indicating that no volume change occurred in the shear zones; these types of shear zones are commonly related to subvertical strike-slip setting (e.g., Kerrich et al., 1980); 2) Volume-loss types indicating that elements decreased during progression from protomylonite to ultramylonite; these shear zones are related to compressional tectonic settings (O'Hara, 1988; Dipple et al., 1990), and 3) Volume-gain types which are related to transtensional tectonic settings (Glazner & Bartley, 1991; Bailey et al. 1994; Hippertt, 1998; Kwon et al., 2009).

As illustrated in Fig. 12B, in the volume-loss shear zones with an increased degree of deformation, both Na$_2$O and SiO$_2$ decrease, whereas in the IVG shear zone, Na$_2$O decreases while SiO$_2$ increas-
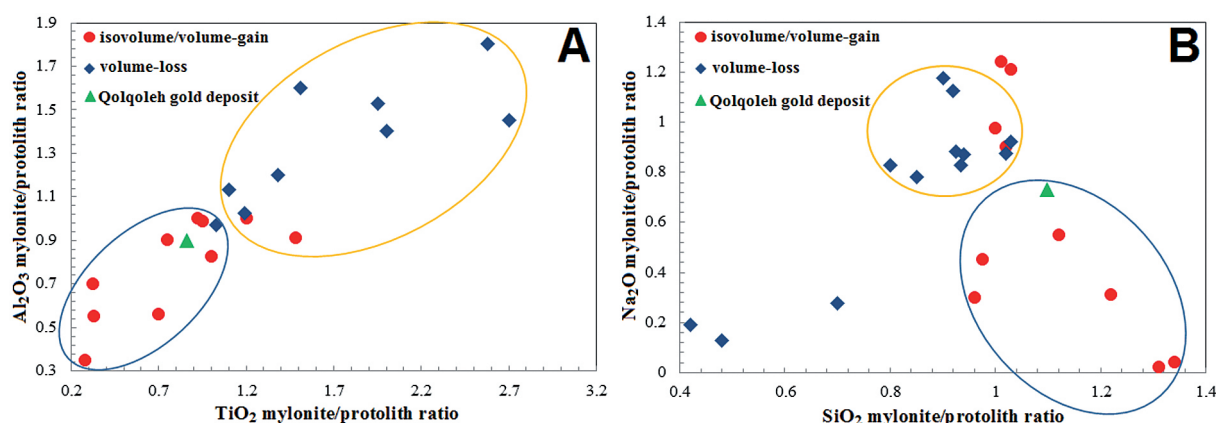
Fig. 12. Two plots of concentration ratios of mylonite/protolith in deformed matavolcanics from shear zones. Red- and blue-marked samples from Candie & Sinha (1996), green-marked ones are average samples from the Qolqoleh gold deposit (the present study).

es. It seems that the decrease in Na_2O and SiO_2 in the volume-loss shear zones is related to feldspar destruction because of passage of large amounts of fluid through shear zones (Glazner & Bartley 1991; Condie & Sinha 1996). In contrast, the IVG ultramylonites often show petrographic evidence of syntectonic silicification. Each type of shear zone can be classified by using the Al_2O_3-TiO_2 diagram (Fig. 12A). These oxides have been enriched in the volume-loss shear zones; whereas the IVG shear zones have been depleted (Condie & Sinha 1996).

The Qolqoleh shear zone is compared with other types of shear zones in the SiO_2-Na_2O and TiO_2-Al_2O_3 diagrams (Fig. 12). By an increased degree of deformation or changing conditions from protomylonite to ultramylonite, SiO_2 increases while Na_2O remains relatively constant (Fig. 12B). Correspondingly, in the Al_2O_3-TiO_2 diagram, by an increased deformation intensity, TiO_2 and Al_2O_3 decrease (Fig. 12A). Based on these diagrams, the shear zone studied is classified as Isovolume-Gain (IVG) type.

6. Fluid inclusion

6.1. Fluid inclusion petrography

Based on the number of phases present at room temperature (Shepherd et al., 1985) and their microthermometric features, three fluid inclusion types were recognised: Type I monophase aqueous inclusions (V), Type II two-phase (liquid+vapour) aqueous inclusions, and Type III three-phase carbonic–aqueous inclusions (liquid water–liquid

CO_2–vapour CO_2). Type II is the most abundant of the three inclusion types. In all types of inclusions, daughter mineral phases were absent.

6.1.1. Monophase aqueous inclusion (Type I)

These types of fluid inclusions occur in both quartz veins and are characterised by one phase (liquid or gas) at room temperature. They are transparent, have a spherical shape and vary in size (3 and 8 µm) (Fig. 13A, B).

6.1.2. Aqueous two-phase fluid inclusions (Type II)

These inclusions are seen in both concordant gold-bearing quartz-sulphide veins, and barren quartz-calcite veins and are characterised by a vapour bubble in an aqueous liquid at room temperature, transparency and low relief. In these inclusions, vapour bubble occupies 25–40% of the total inclusion volume. Morphologically, they show variations from negative crystal to spherical, rectangular, elongate, oval or irregular forms, and their sizes range from 4 to 18 µm (Fig. 13C, D). The primary to pseudosecondary inclusions occur as isolated single or clusters of randomly aligned inclusions.

6.1.3. Carbonic-aqueous inclusions (Type III)

These primary inclusions generally are 5–15 µm in size and consist of three phases, two immiscible liquids (liquid CO_2+ liquid water) and a small CO_2 vapour bubble at room temperature occupying 30% of the total inclusion volume. These inclusions may be irregular, oval or rounded in shape, but are found only in gold-bearing quartz-sulphide veins and veinlets (Fig. 13E, F).
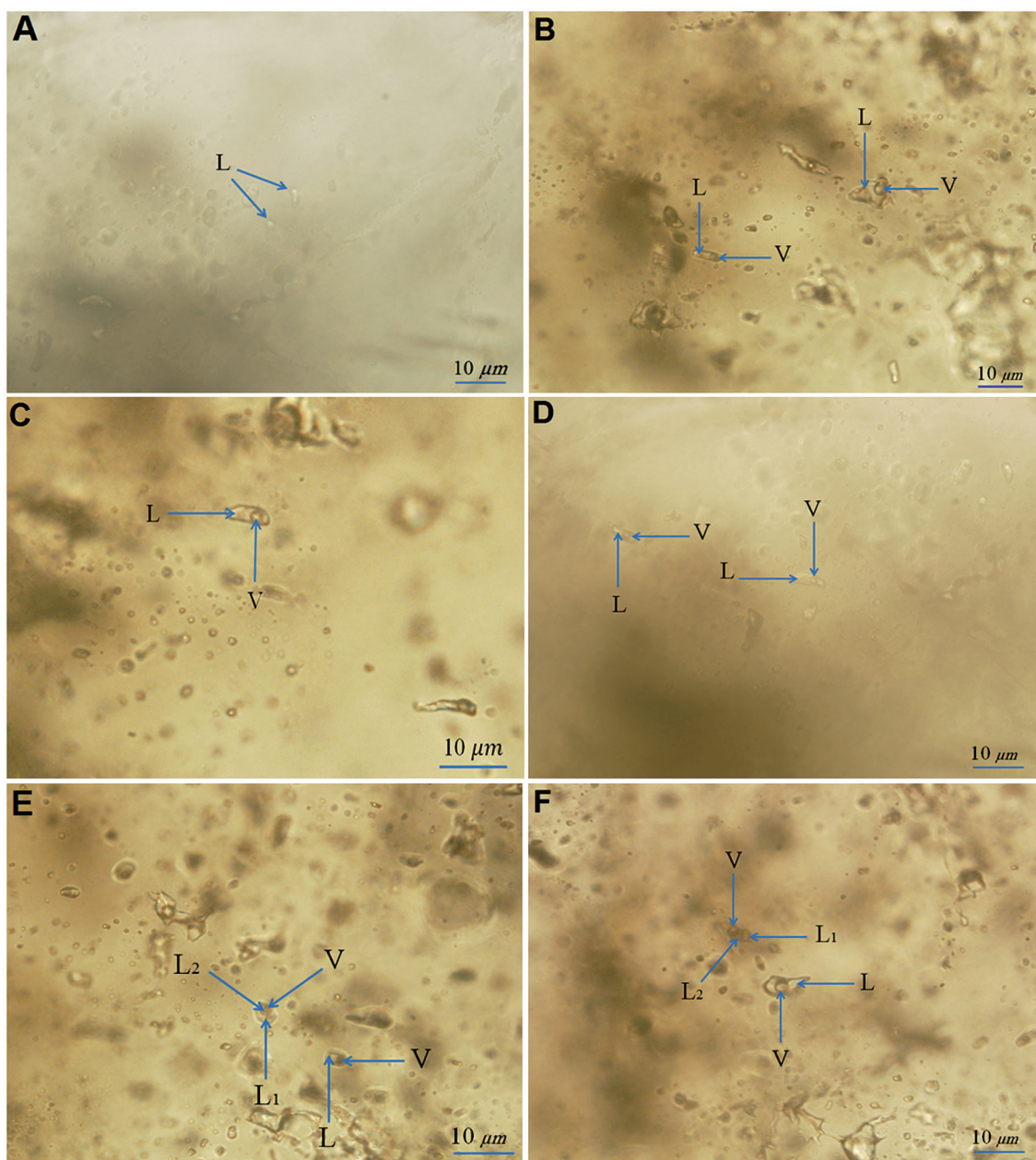
Fig. 13. Petrographic images of fluid inclusion.
A – Type I monophase aqueous fluid inclusion; **B–D** – Type II two-phase aqueous fluid inclusion (L+V); **E, F** – three-phase carbonic aqueous inclusions (Aqueous+LCO$_2$+VCO).

6.2. Fluid inclusion microthermometry

Initial melting of CO$_2$ phase (T$_{M\ CO2}$), CO$_2$ homogenisation (T$_{H\ CO2}$), and final melting of clathrate (T$_{M\ Clath}$) for CO$_2$-bearing inclusions, as well as final melting of ice (T$_{M\ ICE}$) and total homogenisation (T$_{H\ Total}$) for aqueous inclusions were measured (Table 4).

Data obtained from the microthermometric measurements and volume fraction estimates of the phases (for the purpose of transform melting and homogenisation temperatures and optical volume fraction estimates into bulk compositions and densities) were processed using the software packages Fluids (Bakker, 1999) and clathrates (Bakker, 1997). Calculations of salinity for aqueous and carbonic aqueous inclusion, fractions of compositions, density of carbonic liquid and bulk fluid, and bulk molar volume of fluid inclusions were made using the FLINCOR program by Brown (1989). The FLINCOR software and Bodnar (1983) diagram were used for density calculation. For pressure estimates in two-

Table 4. Summary of fluid inclusion data for gold-bearing quartz-sulphide and barren quartz-calcite veins from the Qolqoleh gold deposit.

Inclusion type	Number of inclusions	Size [μm]	TM_{CO2} [°C]	$T_{M\ Clath}$ [°C]	$T_{H\ CO2}$ [°C]	$T_{M\ ICE}$ [°C]	$T_{H\ Total}$ [°C]	Salinity [wt% NaCl]
type II-a (aqueous two-phase)	72	3–8				–9.7 to –3	204 to 255	4.85 to 13.62
type II-b (aqueous two-phase)	43	4–18				–16.2 to –11.2	335 to 386	15.17 to 19.58
type III (carbonic–aqueous)	30	5–15	–58.2 to –56.4	1.3 to 4.7	20.4 to 25.3		345 to 386	9.43 to 13.98

phase aqueous inclusions, the equation states of H_2O in P-T projection were used (Diamond, 2003).

6.2.1. Aqueous two-phase inclusions (Type II)

About 78% of the inclusions studied are aqueous inclusions (L+V). Based on T_H, this type of inclusions is classified into two groups: a) Those with low-intermediate T_h (205–255°C, with a sharp peak at 235°C; Fig. 14A). The $T_{M\ ICE}$ of this type fluid inclusion ranges from –3 to –9°C (Fig. 14B), indicating salinities between 5–13 wt% NaCl equivalent (with a high frequency at 11–12 wt% NaCl equivalent; Fig. 14C) and bulk fluid densities between 0.84 and 0.96 gr/cm³ (Fig. 15). This type of fluid inclusion is the most abundant; and b) High T_h from 335 to 385°C (Fig. 14A) and $T_{M\ ICE}$ from –11 to –16°C (Fig. 14B), indicating salinities between 15 and 19 wt% NaCl equivalent (with a sharp peak at 16 wt% NaCl equivalent; Fig. 14C). Bulk fluid density ranges between 0.79 to 0.86 g/cm³ (Fig. 15).

6.2.2. Carbonic–aqueous inclusions (Type III)

Total homogenisation ($T_{H\ Total}$) into the liquid phase was observed between 345 and 385°C, with a mode at 365°C (Fig. 14A). These inclusions show T_{MCO2} ranging from –56.4 to –58.3°C. Homogenisation of the carbonic phase ($T_{H\ CO2}$), typically to a liquid, was in a narrow range of temperatures between 20.4 and 25.3°C. Melting of the CO_2 clathrate ($T_{M\ Clath}$) in the presence of CO_2 liquid occurred between 1.3 and 4.7°C (Fig. 14B) indicating a salinity of 9–13 wt% NaCl equivalent (Fig. 14C). Bulk fluid densities range between 0.89 and 0.93 gr/cm³ (Fig. 15).

6.3. Pressure condition

Trapping pressure can be estimated from the fluid inclusions trapped under immiscible or boiling conditions or if an independent trapping temperature is known (Brown & Hagemann, 1995). Estimates of trapping pressures for ore-forming fluids in Type II and Type III fluid inclusions were determined using the Touret and Dietvorst (1983) and Diamond (2003) approaches. The highest homogenisation temperature (385°C) is considered as the minimum trapping temperature. The minimum pressure is in the range of 1.6 to 2 kbar (Fig. 16), suggesting that the Qolqoleh gold deposit must have formed at a depth of at least 7.4 km. This depth and the brittle-ductile nature of the ore zones indicate that Qoqoleh constitutes a mesozonal subtype gold deposit (e.g., Groves et al., 1998; Goldfarb et al., 2005).

7. Oxygen and hydrogen isotopes

The gold-bearing quartz-sulphide veins hosted in altered-mineralised metavolcanics and discordant quartz-calcite veins in barren or low-mineralised metavolcanics were analysed for oxygen isotopes (Table 5). Hydrogen isotope analyses were performed on fluid inclusions released from samples of both quartz vein types (Table 5).

Oxygen isotopic compositions of hydrothermal water in equilibrium with quartz were estimated utilising extrapolation of the fractionation formula from Clayton et al. (1972). The fractionation factors were calculated using the mean value of the total homogenisation temperatures of fluid inclusions, plus pressure-corrected temperatures as discussed below. Assuming a quartz-sulphide vein deposition temperature of 369–385°C (based upon the fluid inclusion study outlined above), calculated values for $\delta^{18}O_{fluid}$ approximately ranged between 7‰ and 9‰. In addition, the δD values are from –40.23‰ to –35.27. This is indicative of an isotopically heavy crustal fluid and likely of little involve-
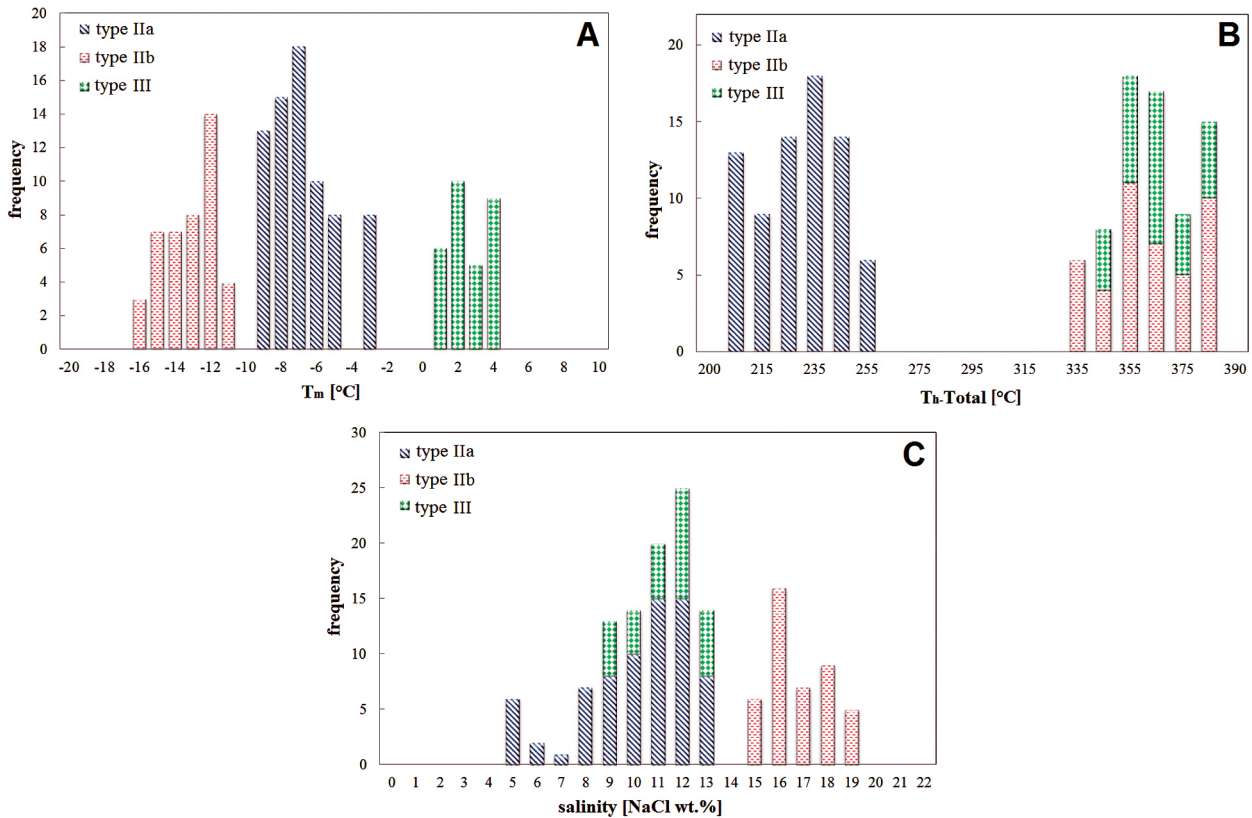
Fig. 14. Fluid inclusion results of quartz veins from the Qolqoleh gold deposit.
  A – Homogenisation temperature; **B** – Melting point of ice and of clathrate; **C** – Salinity of aqueous fluid inclusions
  (type IIa, type IIb) and type III carbonate-aqueous fluid inclusions.
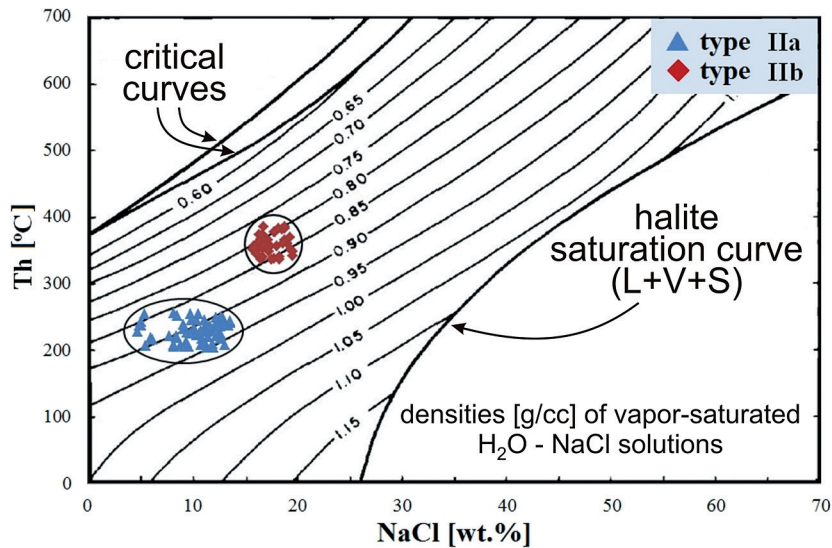

Fig. 15. Salinity-temperature diagram showing density of aqueous fluid inclusions (boundaries after Bodnar, 1983).

ment of meteoric fluid. Sample locations occupy the field of metamorphic fluids (most orogenic gold deposits), and imply involvement of isotopically metamorphic waters during ore formation (Fig. 20). Using temperatures of 249–250°C, the calculated δO^{18} values of water in equilibrium with the late-stage discordant quartz-calcite veins varies from –5.31‰ to –3.35‰, while the δD values range from –5.65‰ to –75.31‰. These values are clearly lower than those of early-stage quartz-sulphide-gold veins, and are close to the meteoric water line.

Table 5. Oxygen and hydrogen isotope compositions (SMOW) for quartz from gold-bearing and barren veins of the Qolqoleh deposit. $\delta^{18}O_{water}$ values are calculated using extrapolation of the fractionation formula from Clayton et al. (1972).

Sample	T_H (°C)	δD ‰	$\delta^{18}O$ ‰	$\delta^{18}O_{water}$
Q 3.32	369	–35.270	12.8	8.010
Q 3.6	385	–40.230	11.6	7.210
Q 2.24	250	–75.310	5.55	–3.350
Q 2.9	249	–95.653	3.6	–5.310
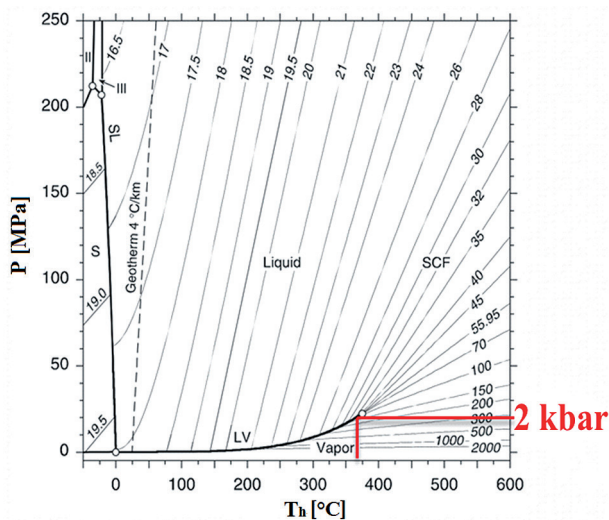
Fig. 16. Temperature-pressure diagram showing pressure during trapping of ore-bearing fluids (boundaries after Diamond, 2003).

8. Discussion

8.1. Hydrothermal alteration and REE mobility

Numerous investigations have been carried out on mobility, fractionation, solubility, and behaviour of REE in hydrothermal and shear zone environments. Rolland et al. (2003) believed that the mobility of REE in the shear zone depended of pH, fO_2, the fluid composition, P-T conditions, and the availability of CO_3^{2-}, PO_4^{2-}, SO_4^{2-}, F^-, and H^- ligands in the fluid. In addition, sulphate complexes (Felsche & Herrmann, 1978), and carbonic fluids (Wendlandt & Harrison, 1979) can control the mobility of REE and preferential fractionation of LREE *vs* HREE. Furthermore, solubility of the REE in hydrothermal systems can be related to carbonate and fluoride complexes (Wood, 1990; Haas et al., 1995). Elevated concentrations of REE may reflect availability of complexing agents, mainly SO_4^{2-} for LREE and F^- for HREE (Rolland et al., 2003). Various ligands may carry and precipitate REE in response to changes in fluid chemistry, due to fluid/rock interaction or fluid mixing processes. The mineralogy and composition of fluid inclusion phases can be used to determine the existence of complexing agents in the hydrothermal fluid. At Qolqoleh, the existence of CO_2-bearing fluid inclusions and carbonate-pyrite association in veins and shear zones indicates the presence of carbonate and sulphur complexes in the mineralising fluid. It seems that LREE enrichment may not be associated with the presence of CO_2 alone (Rolland et al., 2003) and, possibly, sulphate complexes were involved in LREE enrichment because they preferentially form complexes with LREE (Lewis et al., 1997).

It seems that LREE enrichment at Qolqoleh resulted from circulation of SO_4^{2-} and CO_2-bearing fluids due to regional metamorphism in the shear zones. Likewise, the weak fractionation in modified REE patterns (LREE to HREE) could be related to regional effects of metamorphism (greenschist facies) and sericite-chlorite alteration. Geochemical studies show HREE depletion in metavolcanics of the Qolqoleh shear zone. In some cases, HREE enrichment is attributed to decreasing temperature and availability of OH and F-bearing fluids, which could form complexes preferentially with HREE (Haas et al., 1995). HREE depletion may relate to leaching of HREE by F-bearing fluids during increased intensity of hydrothermal alteration at Qolqoleh.

Rolland et al. (2003) thought that changes in REE concentration were related to fluid/rock interaction in shear zones; hence mobility of REE depends of the stability of REE-bearing minerals and thus, directly to fluid. Therefore, considering the low fractionation degree of the REE pattern, the absence of a Eu anomaly and any evidence of fluid/rock interaction in hanging wall and footwall are indicative of any alteration and deformation.

8.2. Eu anomaly

In order to investigate Eu behaviour in the metavolcanics, some samples were taken from ultramylonite and mylonite units. The results indicate the existence of positive and negative Eu anomalies in the mylonite and ultramylonite units, respectively (Fig. 17A, B). It seems that the positive and negative Eu anomalies are correlated with the intensity degree of plagioclase alteration.
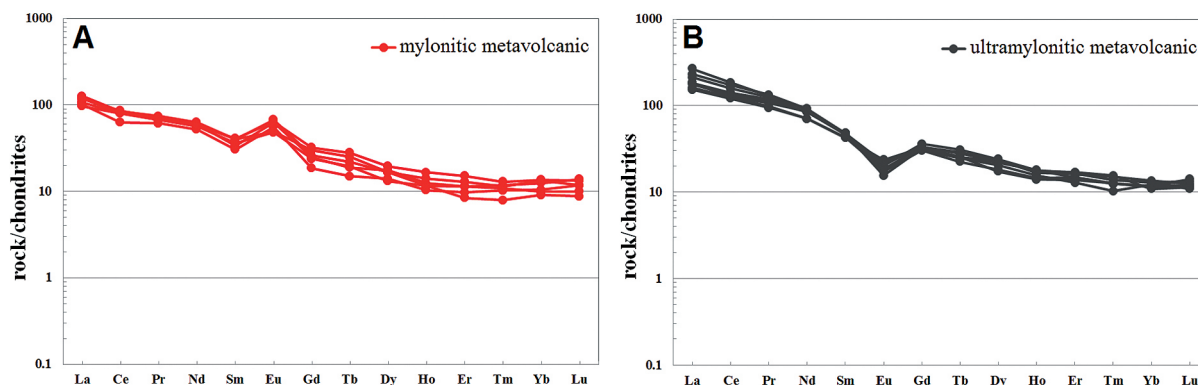
Fig. 17. A – Negative Eu anomaly in highly deformed metavolcanics (ultramylonitic); B – Positive Eu anomaly in less deformed metavolcanics (protomylonitic-mylonitic).
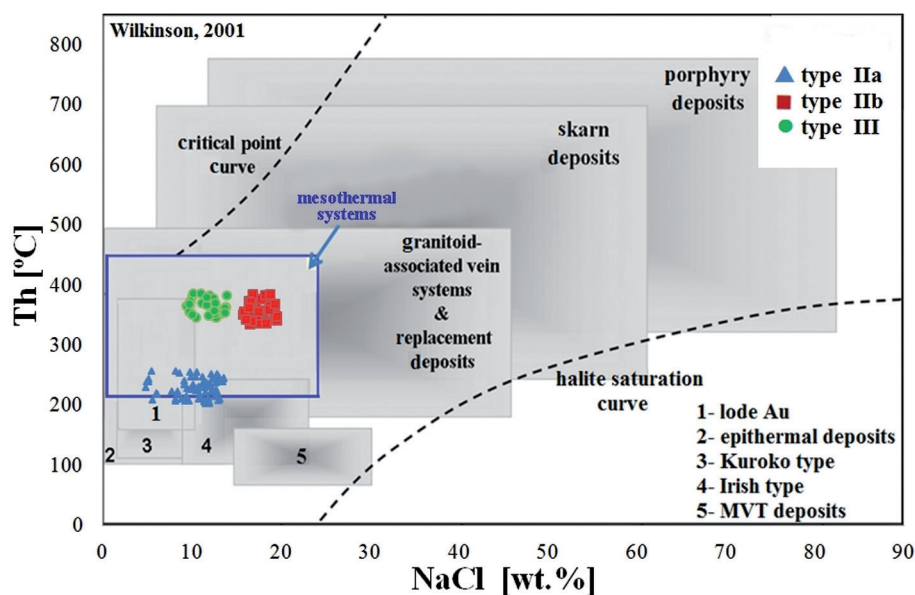

Fig. 18. Temperature-salinity diagram for various types of ore deposits (Wilkinson, 2001). Data from the Qolqoleh deposit plot in the mesothermal deposit field.

The Eu anomalies observed in the REE pattern could be connected to the widespread existence distribution of plagioclase. In mylonitised samples, there is some weak plagioclase alteration to sericite. This could account for the release of some REE from feldspar and mica and REE establishment in secondary sericite. Subsequently, a slight increase in the Eu anomaly (Fig. 17A) and LREE enrichment than HREE are the only chemical changes observed (Schnetzler et al., 1970). Geochemical studies conducted on strongly altered and deformed rocks have shown the role of these agents in the REE distribution pattern.

Increased intensity of deformation in ultramylonite units led to development of microfractures and ores in the rocks, which facilitated fluid flow and ultimately resulted in an increase of the fluid/rock ratio. This process strengthened/boosted

the hydrothermal alteration effect involving feldspars. Therefore, to consider plagioclase as the major carrier and the main source of Eu depletion in these units conforms to the progress of the alteration-deformation process and increasing degree of plagioclase decomposition (Fig. 17B).

8.3. Classification of Qolqoleh gold deposit

The chemistry of vein-forming fluids is remarkably similar in orogenic gold ores of all ages (Groves et al., 2000). Detailed fluid inclusion studies in most greenstone-hosted orogenic Au deposits have shown ore-fluid to contain consistently about 5 mol% CO_2, low salinity H_2O-CO_2±CH_4±N_2 fluid with low H_2S, traces of CH_4 and N_2, and low fO_2 (Groves et al., 1998, 2000; Pirajno, 2009). Orogenic

gold deposits differ from other gold-rich deposit groups in the same terranes, which are formed at uniformly shallow depths (normally 5 km below surface) from highly saline low-CO_2 fluids (e.g. VHMS and porphyry-style deposits) or acidic low-CO_2 fluids (epithermal deposits) and which, characteristically, are either base-metal (±Sn±Mo) and/or silver-enriched (Groves et al., 2000).

The hydrothermal environment of ore-forming fluids at Qolqoleh, based on homogenisation temperature and salinity, was mesothermal (Fig. 18), which, based on a minimum pressure of 1.7–2 kbar, formed at 6.3 to 7.4 km depth (Fig. 16). Based on the tectonic setting of the Qolqoleh area and depth of formation, this deposit is classified as an orogenic gold deposit of the mesozonal subtype (e.g., Groves et al., 1998; Goldfarb et al., 2005). The petrographic and microthermometric characteristics of the fluid inclusions in this type of deposits include small size (>20), low salinity (2 < wt% NaCl < 15) (Roedder, 1984), homogenisation temperature from 300 to 475°C (Groves et al., 1998), H_2O-CO_2±CH_4±N_2-rich fluid inclusions, densities from 0.8 to 1.5 gr/cm^3 (Groves et al., 1998; Goldfarb et al., 2005), gold mineralisation in the brittle-ductile regimes that have undergone greenschist facies metamorphism, and trapping depth for ore-forming fluids (depth of formation) between 6–12 km (Groves et al., 1998). All of these criteria apply to the Qolqoleh gold deposit. Based upon fluid inclusions data, total homogenisation temperature in the gold-bearing quartz-sulphide veins occurred between 335–385°C (Fig. 14A), and the main values of density of ore-forming fluids, pressure and depth of mineralisation are 0.79–0.93 gr/cm^3 (Fig. 15), 1.7–2 kbar, 6.3–7.4 km (Fig. 16), respectively. In addition, the presence of aqueous-carbonic inclusions with low salinity (indicator of metamorphic environments) demonstrates the obvious similarity of fluid inclusions of the Qolqoleh brittle-ductile shear zone to ore-forming fluids in orogenic gold deposits.

8.4. Source of ore-forming fluids

Fluids responsible for gold mineralisation can originate from various sources including magmatic-hydrothermal (Pattrick et al., 1988; De Ronde et al., 2000), metamorphic dehydration (Goldfarb et al., 1991; McCuaig & Kerrich, 1998), meteoric water (Nesbitt et al., 1989; Hagemann et al., 1994), CO_2-rich fluids liberated from the mantle (Cameron, 1988, 1989; Colvine, 1989), or a mixed source of deep-seated magmatic and shallow meteoric water (Zhang et al., 2005).

In the orogenic gold deposits, $\delta^{18}O$ values of hydrothermal fluids are about 5–8 ‰ for Archean greenstone belts, and about 2‰ higher for Phanerozoic gold-bearing belts (Groves et al. 1998). These deposits also show that the δD values range from –30 ‰ to –80‰ (Guilbert & Park 1997). This range is comparable with metamorphic (Burrows & Spooner 1989) and magmatic fluids (So & Yun 1997). Such data from selected orogenic gold deposits are plotted out of the so-called meteoric water (Hagemann et al. 1994) or reaction with organic matter (Goldfarb et al. 1997). Results of stable isotope studies demonstrate the role of different fluids in the genesis of quartz-sulphide and quartz-calcite veins during the evolution of the Qolqoleh gold deposit. The $\delta^{18}O$ and δD values for water in equilibrium with the quartz-sulphide veins plot within the field of metamorphic fluids and orogenic gold deposits (Fig. 19). This suggests that the Qolqoleh ore-mineralising fluids originated from devolatilisation during deep metamorphism. Devolatilisation of these units occurred synchronously with, or postdates, the development of penetrative (ductile) structures such as shear zones, folds, regional penetrative fabrics, and during overprinting brittle deformation (Aliyari et al., 2009).

The $\delta^{18}O$ and δD values of water in equilibrium with the late-stage quartz-calcite veins indicate a meteoric water source (Fig. 19). Such fluids are nearly neutral, with relatively low S contents, temperatures of about 200 to 350°C and low salinity (Kesler, 2005). These criteria are consistent with the mineralogy and fluid inclusion data of the Qolqoleh deposit. Faulting, microfracturing, and jointing provided suitable pathways for fluid migration during the final stages of deformation.

8.5. Tectonic model for Qolqoleh ore formation

Almost all gold occurrences that have been discovered recently in the northwestern SSZ, formed during the late Zagros orogeny complex. Previous studies (Aliyari et al., 2009; Niromand et al., 2011) indicated that the pre-accretionary gold enrichment in this part of the Zargos shear zone could define a more favourable metal source reservoir for later hydrothermal fluids, and thus, suggest a higher prospectivity for a world-class orogenic gold deposit in the northwestern SSZ. Qolqoleh and other Saqqez-Sardasht-Piranshahr gold occurrences are located in a highly deformed area, close to the eastern edge of the Zagros shear zone and along the structurally complex contact between the Precam-
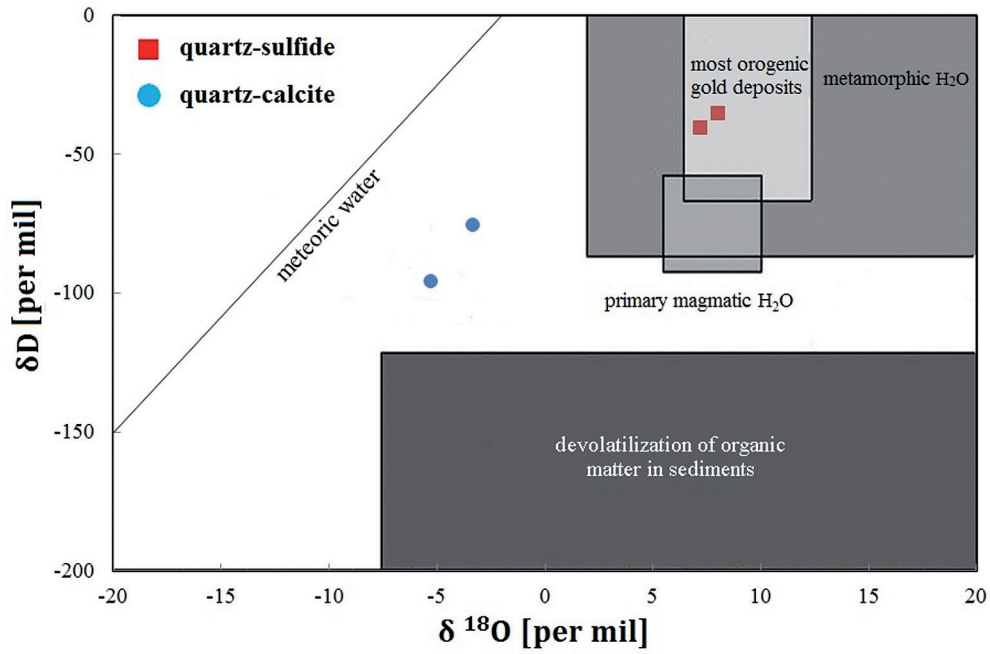
Fig. 19. $\delta^{18}O$ *vs* δD diagram for water in equilibrium with quartz-sulphide and quartz-calcite veins.
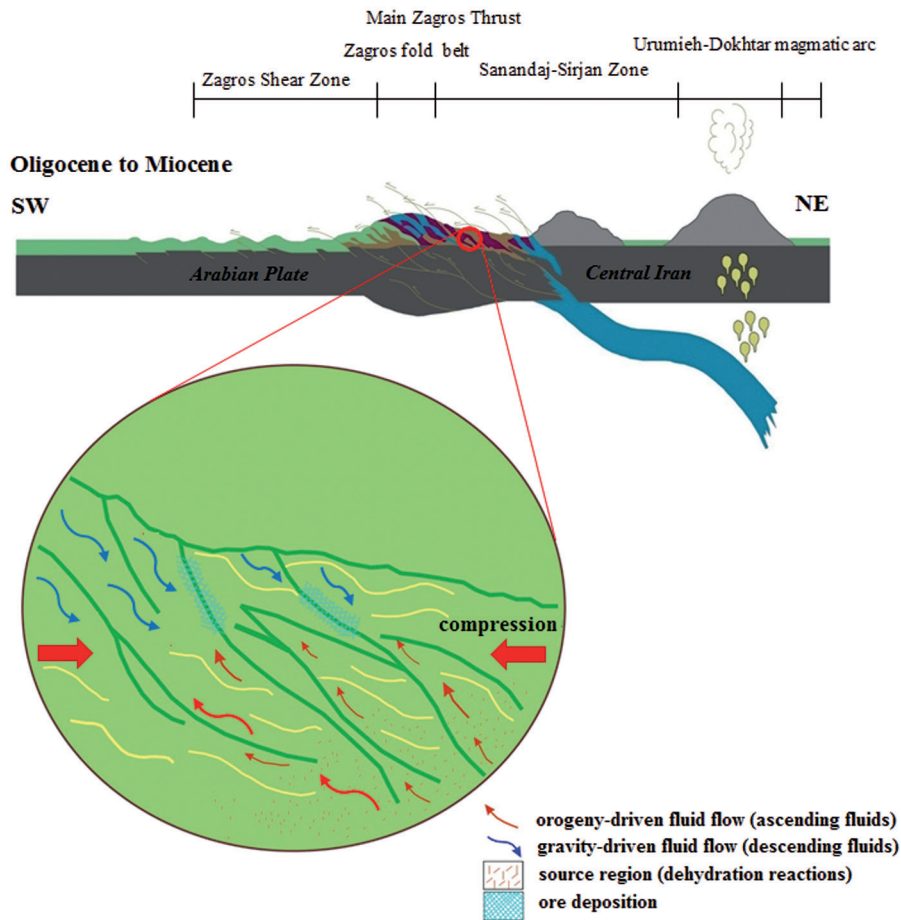

Fig. 20. Conceptual model of gold deposition mechanism in the Qolqoleh shear zone. Extensional conditions which prevailed after orogeny provided an environment conducive to the mobility and migration of ore-bearing fluids. Also circulation of shallow meteoric fluids may have helped in fluid mixing and resulted in deposition of sulphides and gold.

brian basement and the Cretaceous accreted oceanic rocks.

Gold mineralisation in the Qolqoleh deposit, which is controlled by ductile and brittle deformation of the volcano-sedimentary rocks, is developed within structurally controlled dilational fractures. Tectonic setting, isotopic composition and fluid inclusion data suggest that collision-related devolatilisation process during deep metamorphism of the Cretaceous volcano-sedimentary sequences to be the main mechanism of ore fluid formation. Aliyari et al. (2009) argued that metamorphic devolatilisation was focused in boundary areas between the S–SE- and N–NE- trending structural domains and constituted the key factor for the metallogenesis of the orogenic gold deposits in the Sanandaj-Sirjan zone. Accordingly, the volcano-sedimentary sequences progressively deformed during the collision of the Arabian continental and central Iranian microcontinental plates in the Late Jurassic-Early Cretaceous. This compressional tectonic regime led to the formation of a ductile shear zone consisting of protomylonite, mylonite, and ultramylonite. Nevertheless, no significant gold mineralisation occurred during the ductile stage due to a lack of favourable channel ways and insufficient heat energy to drive fluid circulation (Aliyari et al., 2009), until transformation of the tectonic regime from compressional to extensional. During this stage, the uplift of the region induced changes from ductile to brittle regime which in turn caused the distribution of cross structures, fractures, faults, and vein systems. Therefore, changes from compressional to extensional conditions, in association with increasing geothermal gradients (emplacement of intrusive bodies), caused the flow of ascending metamorphic fluids and circulation of gravity-driven fluids (meteoric water), which led to fluid mixing and deposition of sulphide minerals with gold (Fig. 20).

9. Conclusions

The Qolqoleh gold deposit is a ductile to brittle-orogenic deposit within the northwestern part of the Sanandaj–Sirjan metamorphic belt. The rocks in the vicinity of the Qolqoleh deposit predominately consist of Cretaceous volcano-sedimentary sequences of phyllite, meta-limestone, cholorite-sericite schist, metavolcanic and Oligocene granitoid rocks that have undergone greenschist facies metamorphism. Geochemical studies indicate that gold mineralisation occurred in the sulphide-quartz veins.

Fluid-rock interaction during evolution of the Qolqoleh shear zone is commonly associated with changes in major and trace elements chemistry. REE behaviour during hydrothermal fluid-rock interaction in the various rock units shows the existence of strong REE enrichment in metavolcanics of shear zone relative to hanging wall (chlorite-sericite schist) and foot wall (meta-limestone). It seems that LREE enrichment resulted from circulation of SO_4^{2-} and CO_2-bearing fluids due to episodes of regional metamorphism in the shear zones.

Our investigations demonstrate the spatial and temporal relationships between deformation intensity and element distribution in and adjacent to mylonites and ultramylonites in the Qolqoleh shear zone. Mass transfer calculations indicate that chemical changes that occurred during deformation include enrichment of Si, S, Ca, As, Zn, Cu, Au, Ag, Sb, Bi, Pb, Rb, LOI, and LREE, and depletion of Sr, Ba, Na, Eu, Mg, Th, Cr, Co, and Ni. Relatively immobile components include Al, Ti, Fe, Sc, Y, K, U, P, and HREE (except Eu).

A negative correlation was observed between the Eu/Eu* ratio and gold content, whereas a positive correlation was found between the $(La/Yb)_n$ ratio and gold content in mylonitic and ultramylonitic metavolcanics. Mylonitic zones are characterised by a positive Eu anomaly (Eu/Eu* > 1) and lower gold content, whereas ultramylonite units show a negative Eu anomaly (Eu/Eu* < 1) and higher gold content.

Two types of quartz veins are found in the Qolqoleh shear zone: concordant mylonitic quartz-sulphide veins, and discordant mylonitic quartz-carbonate veins. Gold mineralisation occurs in the former. Fluid inclusions microthermometry shows two distinct ranges of homogenisation temperatures (205–255°C and 335–385°C). Both microthermometric and stable isotope data indicate that two types of fluids were involved in the mineralisation, 1) a high-temperature, moderately saline and deep metamorphic fluid which formed quartz-sulphide-gold mineralisation, and 2) low-temperature, low-salinity, meteoric fluid responsible for late-stage quartz-calcite mineralisation.

The Qolqoleh gold mineralisation is of the orogenic type (like other deposits: Mute, Kherapeh and Karavian in the Sanandaj-Sirajn Zone). The Cretaceous volcano-sedimentary sequences of the Saqqez-Sardasht-Piranshahr zone which hosts gold deposits was progressively deformed during the continental collision of the Arabian Plate with the Iranian microcontinent. This deformation was accompanied by plutonism and greenschist facies metamorphism. No significant gold mineralisation

occurred during ductile deformation and compressional tectonic regime due to a lack of favourable channel ways and insufficient heat energy to drive fluid circulation (Aliyari et al., 2009). Major gold mineralisation took place when the tectonic regime transformed from compressional to extensional system. In this zone, changes from compressional to extensional regimes, combined with increasing geothermal gradients (emplacement of intrusive bodies), induced remobilisation of considerable amounts of metamorphic fluids and finally deposited sulphide minerals with gold mineralisation.

Acknowledgments

References

Agard, P., Omrani, J., Jolivet, L. & Mouthereau, F., 2005. Convergence history across Zagros (Iran): constraints from collisional and earlier deformation. *International Journal of Earth Sciences* 94, 401–419.

Alavi, M., 1994. Tectonics of the Zagros orogenic belt of Iran: new data and interpretations. *Tectonophysics* 229, 211–238.

Alavi, M., 2004. Regional stratigraphy of the Zagros folded-thrust belt of Iran and its proforeland evolution. *American Journal of Science* 304, 1–20.

Alavi, M., 2007. Structures of the Zagros fold-thrust belt in Iran. *American Journal of Science* 307, 1064–1095.

Aliyari, F., Rastad, E. & Zengqian, H., 2007. Orogenic gold mineralization in the Qolqoleh gold deposit, Northwestern Iran. *Resource Geology* 57, 262–289.

Aliyari, F., Ebrahim, R., Mohammad, M. & Greg, B.A., 2009. Geology and geochemistry of D–O–C isotope systematics of the Qolqoleh gold deposit, Northwestern Iran: Implications for ore genesis. *Ore Geology Reviews* 36, 306–314.

Aliyari, F., Ebrahim, R., Goldfarb, R. & Sharif, j.A., 2012. Geochemistry of hydrothermal alteration at the Qolqoleh gold deposit in the northern part of the Sanandaj-Sirjan metamorphic belt, northwestern Iran. *Journal of Geochemical Exploration* DOI: 10.1016/j.gexplo.2012.02.001.

Arvin, M., Pan, Y., Dargahi, S., Malekizadeh, A. & Babaei, A., 2007. Petrochemistry of the Siah–Kuh granitoid stock southwest of Kerman, Iran: implications for initiation of Neotethys subduction. *Journal of Asian Earth Sciences* 30, 474–489.

Azizi, H. & Moinevaziri, H., 2009. Review of the tectonic setting of Cretaceous to Quaternary volcanism in northwestern Iran. *Journal of Geodynamics* 47, 167–179.

Baharifar, A., Moinevaziri, H., Bellon, H. & Pique, A., 2004. The crystalline complexes of Hamadan (Sanandaj-Sirjan Zone, western Iran): metasedimentary Mesozoic sequences affected by late Cretaceous tectono-metamorphic and plutonic events. *Comptes Rendus Geoscience* 336, 1443–1452.

Bailey, C.M., Simpson, C. & De Paor, D.G., 1994. Volume loss and tectonic flattening strain in granitic mylonites from the Blue Ridge province, central Appalachians. *Journal of Structural Geology* 16, 1403–1416.

Bakker, R.J., 1997. Clathrates: computer programs to calculate fluid inclusion V–X properties using clathrate melting temperatures. *Computer Geosciences* 23, 1–18.

Bakker, R.J., 1999. *Optimal interpretation of microthermometrical data from fluid inclusions: thermodynamic modeling and computer programming*. Ruprecht-Karls University, Heidelberg, 50 pp. (in German)

Bau, M., 1991. Rare-earth elements mobility during hydrothermal and metamorphic fluid-rock interaction and the significance of the oxidation state of Europium. *Chemical Geology* 93, 219–230.

Berberian, M., 1976. *Seismotectonic Map of Iran*, 1:2500000. Geological Survey of Iran.

Berberian, F. & Berberian, M., 1981. Tectono-plutonic episodes in Iran. [In:] Gupta, H.K. & Delany, F.M. (Eds), *Zagros–Hijndu Kush–Himalaya geodynamic evolution*. American Geophysical Union, Geodynamic Series 3, 5–32.

Berberian, M. & King, G.C.P., 1981. Towards a paleogeography and tectonic evolution of Iran. *Canadian Journal of Earth Sciences* 18, 210–26.

Berberian, M., 1983. The Southern Caspian: A Compressional Depression Floored by a Trapped, Modified Oceanic Crust. *Canadian Journal of Earth Sciences* 20, 163–83.

Berberian, M., 1995. Master blind thrust faults hidden under the Zagros folds: active basement tectonics and surface morphotectonics. *Tectonophysics* 241, 193–224.

Bierlein, F.P., Hughes, M., Dunphy, J., McKnight, S., Reynolds, P.R. & Waldron, H.M., 2001. Trace element geochemistry, 40Ar/39Ar ages, Sm–Nd

systematics and tectonic implications of mafic-intermediate dykes associated with orogenic lode gold mineralisation in central Victoria, Australia. *Lithos* 58, 1–31.

Bodnar, R.J., 1983. A method of calculating fluid inclusion volumes based on vapor bubble diameters and P-V-T-X properties on inclusion fluid. *Economic Geology* 78, 535–542.

Brown, P.E., 1989. FLINCOR: A microcomputer program for the reduction and investigation of fluid-inclusion data. *American Mineralogist Journal* 74, 1390–1393.

Brown, P.E. & Hagemann, S.G., 1995. MacFlincor and its application to fluids in Archean lode-gold deposits. *Geochimica et Cosmochima Acta* 59, 3943–3952.

Burrows, D.R. & Spooner, E.T.C ., 1989. Pb isotope geochemistry of the Silidor and Launay gold deposits; implications for the source of Archean Au in the Abitibi Subprovince. *Economic Geology* 88, 1722–1730.

Cameron, E.M., 1988. Archean gold: relation to granulite formation and redox zoning in the crust. *Geology* 16, 109–112.

Cameron, E.M., 1989. Scouring of gold from the lower crust. *Geology* 17, 26–29.

Clayton, R.N., O,Neil, L.R. & Mayeda, T.K., 1972. Oxygen isotope exchange between quartz and water. *Journal of Geophysical Research* 77, 3057–3067.

Colvine, A.C., 1989. An empirical model for the formation of Archean gold deposits: Products of final cratonization of the Superior Province, Canada, [In:] Keys, R.R., Ramsay, W.R.H. & Groves, D.I. (Eds), *The Geology of Gold Deposits: The Perspective in 1988*. Economic Geology Monograph 6, 37–53.

Condie, K.C. & Sinha, A.K., 1996. Rare earth and other trace element mobility during mylonitization: a comparison of the Brevard and Hope Valley shear zones in the Appalachian mountains, USA. *Journal of Metamorphic Geology* 14, 213–226.

De Ronde, C.E.J., Faure, K., Bray, C.J. & Whitford, D.J., 2000. Round Hill shear zone-hosted gold deposit, Macraes flat, Otago, New Zealand: evidence of a magmatic ore fluid. *Economic Geology* 95, 1025–1048.

Diamond, L.W., 2003. Systematics of H2O inclusions. [In:] Samson, I., Anderson, A. & Marshall, D. (Eds) *Fluid Inclusions: Analysis and Interpretation*. Mineralogical Association of Canada, Short Course 32, 55–79.

Dickin, A.P., 1988. Evidence for limited REE leaching from the Roffna Gneiss, Switzerland – a discussion of the paper by Vocke et al. *Contributions to Mineralogy and Petrology* 99, 273–275.

Dipple, G.M., Wintsch, R.P. & Andrews, M.S., 1990. Identification of the scales of differential element mobility in a ductile shear zone. *Journal of Metamorphic Geology* 8, 645–661.

Eftekhar-Nezhad, J., 1973. *The Mahabad Quadrangle Map, 1:250000*. Geological Survey and Mineral Exploration of Iran.

Eftekhar-Nezhad, J., 1981. Tectonic division of Iran with respect to sedimentary basins. *Journal of Iranian Petroleum Society* 82, 19–28 (in Farsi).

Felsche, J. & Herrmann, A.G., 1978. Yitrium and lanthanides. [In:] Wedpohl, K. (Ed.), *Handbook of Geochemistry*. Springer-Verlag, New York, 57–71.

Fourcade, S., Marquer, D. & Javoy, M., 1989. 18O/16O variations and fluid circulation in a deep shear zone: the case of the alpine ultramylonites from the Aar massif (Central Alps, Switzerland). *Chemical Geology* 77, 119–131.

Ghasemi, A. & Talbot, C.J., 2006. A new tectonic scenario for the Sanandaj–Sirjan Zone (Iran). *Journal of Asian Earth Sciences* 26, 683–693.

Glazner, A.F. & Bartley, J.M., 1991. Volume loss fluid flow and state of strain in the extensional mylonites from the central Mojave Desert, California. *Journal of Structural Geology* 5, 587–594.

Goddard, J.V. & Evans, J.P., 1995. Chemical changes and fluid–rock interaction in faults of crystalline thrust sheets, northwestern Wyoming, USA. *Journal of Structural Geology* 17, 533–547.

Goldfarb, R.J., Groves, D.I. & Gardoll, S., 2001. Orogenic gold and geologic time: a global synthesis. *Ore Geology Reviews* 18, 1–75.

Goldfarb, R.J., Ayuso, R., Miller, M.L., Ebert, S.W., Marsh, E.E., Petsel, S.A., Miller, L.D., Bradley, D., Johnson, G. & Mcclelland, W., 2004. The Late Cretaceous Donlin Creek Gold Deposit, Southwestern Alaska: Controls on Epizonal Ore Formation. *Economic Geology* 99, 643–671.

Goldfarb, R.J., Baker, T., Dube, B., Groves, D.I., Hart, C.J.R. & Gosselin, P., 2005. *Distribution, character and genesis of gold deposits in metamorphic terranes*. Economic Geology 100th Anniv., 407–450.

Grant, J.A., 1986. The isocon diagram – a simple solution to Gresens' equation for metasomatic alteration. *Economic Geology* 81, 1976–1982.

Grant, J.A., 2005. Isocon analysis: A brief review of the method and applications. *Physics and Chemistry of the Earth* 30, 997–1004.

Gresens, R.L., 1967. Composition–volume relationships of metasomatism. *Chemical Geology* 2, 47–65.

Groves, D.I., Goldfarb, R.J., Gebre, M.M., Hagemann, S.G. & Robert, F., 1998. Orogenic gold

deposits: a proposed classification in the context of their crustal distribution and relationship to other gold deposit types. *Ore Geology Reviews* 13, 7–27.

Groves, D.I., Goldfarb, R.J., Knox-Robinson, C.M., Ojala, J., Gardoll, S., Yun, G. & Holyland, P., 2000. Late-kinematic timing of orogenic gold deposits and significance for computer-based exploration techniques with emphasis on the Yilgarn block, Western Australia. *Ore Geology Reviews* 17, 1–38.

Guilbert, J.M. & Park, C.F., 1997. *The geology of ore deposits*. W. H. Freeman and Company, New York, 985pp.

Haas, J.R., Shock, E.L. & Sassani, D.C., 1995. Rare earth elements in hydrothermal systems: estimates of standard partial molal thermodynamic properties of aqueous complexes of the rare earth elements at high pressures and temperatures. *Geochimica et Cosmochimica Acta* 59, 4329–4350.

Hagemann, S.G., Gebre-Mariam, G. & Groves, D.L., 1994. Surface-water influx in shallow-level Archean lode gold deposits in Western Australia. *Geology* 22, 1067–1070.

Hippertt, J.F., 1998. Breakdown of feldspar, volume gain and lateral mass transfer during mylonitization of granitoid in a low metamorphic grade shear zone. *Journal of Structural Geology* 20, 175–193.

Ingles, J., Lamouroux, C., Soula, J.C., Guerrero, N. & Debat, P., 1999. Nucleation of ductile shear zone in a granodiorite under greenschist facies conditions, Néouvielle massif, Pyrenees, France. *Journal of Structural Geology* 21, 555–576.

Irvine, T.N. & Baragar, W.R.A., 1971. A guide to the chemical classification of the common volcanic rocks. *Canadian Journal of Earth Sciences* 8, 523–548.

Kerrich, R., Allison, I., Barnett, R.L., Moss, S. & Starkey, J., 1980. Microstructural and chemical transformations accompanying deformation of granite in a shear zone at Mieville, Switzerland; with implications for stress corrosion cracking and superplastic flow. *Contributions to Mineralogy and Petrology* 73, 221–241.

Kesler, S.E., 2005. Ore-forming fluids. *Elements* 1, 13–18.

Kikawada, Y., 2001. Experimental studies on the mobility of lanthanides accompanying alteration of andesite by acidic hot spring water. *Chemical Geology* 176, 137–149.

Kwon, S., Park, Y., Park, C. & Kim, H.S., 2009. Mass-balance analysis of bulk-rock chemical changes during mylonitization of a meg-acryst-bearing granitoid, Cheongsan shear zone, Korea. *Journal of Asian Earth Sciences* 35, 489–501.

Lewis, A.J., Palmer, M.R., Sturchio, N.C. & Kemp, A.J., 1997. The rare earth element geochemistry of acid-sulphate and acid-sulphate-chloride geothermal systems from Yellowstone National Park, Wyoming, USA. *Geochimica et Cosmochimica Acta* 61, 695–706.

Lottermoser, B.G., 1992. Rare earth elements and hydrothermal ore formation processes. *Ore Geology Reviews* 7, 25–41.

McCuaig, T.C. & Kerrich. R., 1998. P-T-t-deformation-fluid characteristics of lode gold deposits: evidence from alteration systematics. *Ore Geology Reviews* 12, 381–453.

Michard, A., 1989. Rare earth element systematic in hydrothermal fluid. *Geochimica et Cosmochimica Acta* 53, 745–750.

Mohajjel, M., 1997. Structure and tectonic evolution of Palaeozoic-Mesozoic rocks, Sanandaj-Sirjan Zone, Western Iran. University of Wollongong, Wollongong, 284 pp.

Mohajjel, M., 2000. *Geological map of the Qolqoleh and Kervian gold deposits, 1:5000*. Geological Survey of Iran.

Mohajjel, M., Fergusson, C.L. & Sahandi, M.R., 2003. Cretaceous–Tertiary convergence and continental collision, Sanandaj–Sirjan Zone, western Iran. *Journal of Asian Earth Sciences* 21, 397–412.

Moinevaziri, H., 1985. *Volcanisme Tértiaire et Quatérnaire en Iran*. [Tertiary and Quaternary volcanism in Iran]. University Paris-Sud, Paris, 290 pp. (in French)

Murray, R.W., Brink, M.R., Jones, D.L., Gerlach, D.C. & Russ, G.P., 1990. REE as indicators of deffrent marine depositional environments in chert and shale. *Geology* 18, 268–271.

Nakamura, N., 1974. Determination of REE, Ba, Fe, Mg, Na and K in carbonaceous and ordinary chondrites. *Geochimical Acta* 38, 757–775.

Nesbitt, B.E., Muehlenbachs, K. & Murrowchick, J.B., 1989. Genetic implications of the stable isotope characteristics of mesothermal Au deposits and related Sb and Hg deposits in the Canadian Cordillera. *Economic Geology* 84, 1489–1506.

Newman, J. & Mitra, G., 1993. Lateral variations in mylonite zone thickness as influenced by fluid–rock interactions, Linville Falls fault, North Carolina. *Journal of Structural Geology* 15, 849–863.

Niroomand, S., Goldfarb, R.J., Moore, F., Mohajjel, M. & Marsh, E.E., 2011. The Kharapeh orogenic gold deposit: geological, structural, and geochemical controls on epizonal ore formation in West Azerbaijan Province, Northwestern Iran. *Mineralium Deposita* 46, 409–428.

O'Hara, K., 1988. Fluid flow and volume loss during mylonitization: an origin for phyllonites in an overthrust setting, North Carolina. USA. *Tectonophysics* 156, 21–36.

O'Hara, K. & Blackburn, W.H., 1989. Volume-loss model for trace-element enrichments in mylonites. *Geology* 17, 524–527.

O'Hara, K., 1990. State of strain in mylonites from the western Blue Ridge province, southern Appalachians: the role of volume loss. *Journal of Structural Geology* 12, 419–430.

Omrani, J., Agard, P., Whitechurch, H., Mathieu, B., Prouteau, G. & Jolivet, L., 2008. Arc-magmatism and subduction history beneath the Zagros Mountains, Iran. A new report of adakites and geodynamic consequences. *Lithos* 106, 380–398.

Pattrick, R.A.D., Boyce, A. & MacIntyre, R.M., 1988. Gold and silver mineralization at Tyndrum, Scotland. *Mineralogy and Petrology* 38, 61–76.

Pearce, J.A., Harris, N.W. & Tindle, A.G., 1984. Trace element discrimination diagrams for the tectonic interpretation of granitic rocks. *Journal of Petrology* 25, 956–983.

Pirajno, F., 2009. *Hydrothermal mineral deposits, principle and fundamental concept for the exploration geologist*. Springer, 706 pp.

Roedder, E., 1984. Fluid inclusions. *Reviews in Mineralogy* 12, 644.

Rolland, Y., Cox, S., Boullier, A.M., Pennacchioni, G. & Mancktelow, N., 2003. Rare earth and tracen element mobility in mid-crustal shear zones: insights from the Mont Blanc Massif (Western Alps). *Earth and Planetary Science Letters* 214, 203–219.

Rollinson, H.R., 1993. *Using geochemical data: evolution, presentation, interpretation*. Longman, London, 652 pp.

Sarkarinejad, K. & Alizadeh, A., 2009. Dynamic model for the exhumation of the Tutak gneiss dome within a bivergent wedge in the Zagros Thrust System of Iran. *Journal of Geodynamics* 47, 201–209.

Selverstone, J., Morteani, G. & Stuade, J.M., 1991. Fluid channelling during ductile shearing: transformation of granodiorite into aluminous schist in the Tauern Window, eastern Alps. *Journal of Metamorphic Geology* 9, 419–431.

Shahabpour, J., 2005. Tectonic evolution of the orogenic belt in the region located between Kerman and Neyriz. *Journal of Asian Earth Sciences* 24, 405–17.

Sheikholeslami, M.R., Pique, A., Mobayen, P., Sabzehei, M., Bellon, H. & Hashem Emami, M., 2008. Tectono-metamorphic evolution of the Neyriz metamorphic complex, Quri-Kor-e-Sefid area (Sanandaj– Sirjan Zone, SW Iran). *Journal of Asian Earth Sciences* 31, 504–521.

Shepherd, T.J., Rankin, A.H. & Alderton, D.H.M., 1985. *A Practical Guide to Fluid Inclusion Studies*. Blackie, Glasgow, 239 pp.

Sinha, A.K., Hewitt, D.A. & Rimstidt, J.D., 1986. Fluid interaction and element mobility in the development of ultramylonites. *Geology* 14, 883–886.

So, C.S. & Yun, S.T., 1997. Jurassic mesothermal gold mineralization of the Samhwanghak mine, Youngdong area, Republic of Korea: constraints on hydrothermal fluid chemistry. *Economic Geology* 92, 60–80.

Sterner, S.M. & Bodnar, R.J., 1984. Synthetic fluid inclusions in natural quartz. I. Compositional types synthesized and applications to experimental geochemistry. *Geochimica et Cosmochimica Acta* 48, 2659–2668.

Taylor, S.R. & McLennan, S.M., 1985. *The Continental Crust: its Composition and Evolution*. Blackwell, Oxford, 312 pp.

Touret, J. & Dietvorst, P., 1983. Fluid inclusions in high-grade anatectic metamorphites. *Journal of the Geological Society of London* 140, 635–649.

Touret, J.L.R., 2001. Fluids in metamorphic rocks. *Lithos* 55, 1–26.

Vance, R.K. & Condie, K.C., 1987. Geochemistry of footwall alteration associated with the early Proterozoic United Veerde massive sulfide deposit, Jerome, Arizona. *Economic Geology* 82, 571–586.

Wendlandt, R.F. & Harrison, W.J., 1979. Rare earth partitioning between immiscible carbonate and silicate liquids and CO_2 vapour: results and implications for the formation of light rare-earth-enriched rocks. *Contributions to Mineralogy and Petrology* 69, 409–419.

Wilkinson, J.J., 2001. Fluid inclusions in hydrothermal ore deposits. *Lithos* 55, 229–272.

Wood, S.A., 1990. The aqueous geochemistry of the rare-earth elements and Yttrium. 2. Theoretical predictions of speciation in hydrothermal solutions to 350°C at saturation water vapour pressure. *Chemical Geology* 88, 99–125.

Zhang, X.H., Liu, Q., Ma, Y.J. & Wang, H., 2005. Geology, fluid inclusions, isotope geochemistry, and geochronology of the Paishanlou shear zone-hosted Gold Deposit, North China Craton. *Ore Geology Reviews* 26, 325–348.